Towards improved spatio-temporal resolution soil moisture retrievals from the synergy of SMOS and MSG SEVIRI spaceborne observations

Piles, M.; Petropoulos, George; Sánchez , Nilda; González-Zamora, Ángel; Ireland, Gareth; Miles, María

Published in:
Remote Sensing of Environment

DOI:
10.1016/j.rse.2016.02.048

Publication date:
2016

Citation for published version (APA):
Piles, M., Petropoulos, G., Sánchez , N., González-Zamora, Á., Ireland, G., & Miles, M. (2016). Towards improved spatio-temporal resolution soil moisture retrievals from the synergy of SMOS and MSG SEVIRI spaceborne observations. *Remote Sensing of Environment*, *180*, 403-417. https://doi.org/10.1016/j.rse.2016.02.048

Towards improved spatio-temporal resolution soil moisture retrievals from the synergy of SMOS and MSG SEVIRI spaceborne observations

María Piles[1,*], George P. Petropoulos[2], Nilda Sánchez[3], Ángel González-Zamora[3], Gareth Ireland[2]

[1]*Department of Signal Theory and Communications, Universitat Politècnica de Catalunya, and SMOS Barcelona Expert Center, Pg. Maritim de la Barceloneta 37-49, 08003 Barcelona, Spain*

[2]*Department of Geography and Earth Sciences, University of Aberystwyth, SY23 2EJ, UK*

[3] *Instituto Hispano Luso de Investigaciones Agrarias (CIALE), Universidad de Salamanca (USAL), Duero 12, E-37185 Villamayor, Spain*

*Author of correspondence: maria.piles@tsc.upc.edu; Tel: +34 93 230 96 31, Fax: +34 93 230 95 55

Abstract

Earth Observation (EO) technology is today at a maturity level that allows deriving operational estimates of Surface Soil Moisture (SSM) from a variety of sensors; yet, such products are at present provided at a coarse spatial and/or temporal resolution, which restricts their use in local or regional scale studies and practical applications. Herein, a methodology to derive SSM estimates from space at previously unattained spatio-temporal resolutions is proposed. The method is based on a variant of the "triangle" inversion technique leveraging on the strengths and synergies of SMOS (Soil Moisture and Ocean Salinity mission) microwave observations and geostationary optical/infrared data. The SSM retrieval technique allows for: i) enhancing the spatial resolution of SMOS SSM product estimates to 3 km spatial resolution, and, ii) providing a temporal average daytime SM product from the instantaneous fine-scale SSM estimates acquired every 15 minutes; the latter is allowing higher coverage in presence of clouds and representativeness (up to 96 estimates per day) in comparison to the instantaneous estimate at the time of satellite overpass.

The proposed technique has been implemented to SMOS and MSG (Meteosat Second Generation) SEVIRI (Spinning Enhanced Visible and Infrared Imager) observations acquired over the Iberian Peninsula and Southern France during year 2011. SSM instantaneous estimates at the time of SMOS overpass and daytime-averaged SSM estimates have been obtained and evaluated separately against collocated in-situ measurements acquired from a total of 40 stations belonging to the REMEDHUS, VAS and SMOSMANIA permanent soil moisture measurement networks. Statistical agreement between compared datasets has been evaluated both at individual stations and considering the network average on the basis of several statistical terms computed including correlation, bias, root-mean-squared errors and slope and intercept of linear regression. Results showed that the proposed method not only preserves the quality of SMOS SSM at finer spatial scales, but also allows achieving higher temporal coverage and representativeness in daytime averages. The synergy of SMOS and SEVIRI provides a pathway to enhance water cycle EO capabilities taking full advantage of the new observational records of SSM and operational geostationary information.

Keywords: *soil moisture, SMOS, MSG SEVIRI, synergy, downscaling, temporal resolution, spatial resolution*

1. **INTRODUCTION**

Accurate monitoring of Earth's terrestrial water and energy cycles is today critically important to many hydrological applications such as global food production, assessment of water resources sustainability, flood, drought, and climate change prediction [Wood et al., 2011]. In this regard, global information on the spatio-temporal variation of parameters such as surface soil moisture (SSM) is of key significance. SSM is a key state variable of the hydrological cycle that governs most physical processes dominant in the Earth system and exerts a strong control not only on the water cycle but also in ecosystem functioning [Riveros-Iregui et al., 2012; Shen et al., 2014]. It controls the partitioning of available energy at the ground surface into sensible and latent heat exchange through evaporation and transpiration processes and on the allocation of precipitation into runoff, subsurface flow and infiltration [Petropoulos et al., 2014; GOSIC 2015]. Changes in soil moisture may also have a very serious impact on agricultural productivity, forestry, and ecosystem health. Monitoring SSM is therefore critical in both managing natural resources and in improving our understanding of land surface physical processes and Earth system interactions. Thus, justifiably, being able to provide accurate information on the spatio-temporal variability of SSM is of paramount importance [North et al., 2015].

In the last few decades, Earth Observation (EO) technology has played an increasingly important role in determining SSM. There have been many efforts to obtain an accurate understanding of soil moisture distribution at different spatial and temporal scales, utilising information from different types of spaceborne sensors [Zhao and Li, 2013, see also recent review by Petropoulos et al., 2015]. There are at present three globally distributed operational products for the retrieval of SSM from space, which all exploit EO data acquired from microwave instruments. The European Space Agency's (ESA) Soil Moisture and Ocean Salinity (SMOS) mission is the first passive L-band microwave space mission dedicated to globally measure the Earth's SSM. Since the end of 2009, it provides ~ 35 km SSM estimates every 3 days with a target accuracy of 0.04 $m^3 m^{-3}$. The spatial resolution of SMOS is adequate for many global applications, but restricts the use of the data in regional studies over land, where a resolution of 1–10 km is needed [Piles et al., 2011]. Soil moisture information is also being retrieved from active microwave sensors, specifically from ESA's Advanced Scatterometer (ASCAT), which was launched in 2006 aboard MetOp-A satellite [Oschner et al., 2013]. ASCAT is a C-band active radar operating at 5.255 GHz which produces SSM estimates with a spatial resolution of 50 km and 25 km (resampled to 25 km and 12.5 km grids in the swath geometry), and a temporal resolution of 3 days [Wagner et al., 2013]. However, C-band observations are not optimal for soil moisture retrieval as they are sensitive to a shallower soil layer than L-band observations and are more significantly affected by vegetation attenuation [Panciera et al., 2014]. The recently launched Soil Moisture Active Passive (SMAP) satellite utilises combined passive (radiometer) and active (radar) microwave instruments at L-band to provide measurements of near-surface soil moisture (0–5 cm depth) and land freeze/thaw condition over a 1000 km swath with a global revisit of 2–3 days. The dual sensor SMAP profits from the specific advantages of each microwave instrument, allowing for a higher spatio-temporal resolution SSM dataset in comparison to either individual passive (typically coarse resolution) or active (typically low temporal resolution) sensors. However, operations of active-passive products ceased abruptly with the failure of the SMAP radar after about ten weeks of operations.

Despite the breadth of EO sensors currently in orbit and the promising accuracies reported by different techniques measuring SSM from space, the primary challenges in using existing operational SSM data remain. Perhaps the key challenge is that the spatial and/or temporal support volumes do not sufficiently represent the spatio-temporal dynamics/variations and uncertainties of SSM at small scales [Oschner et al., 2013; Barrett and Petropoulos, 2013]. Many hydrological applications require

information on soil moisture at sub-daily temporal resolutions, where this time-dependent data is needed to initialise and update forecast, storm water management, flood or hydrological models. Therefore, there is a requirement for the development of EO synergistic approaches that allow providing SSM information at the requisite spatio-temporal scale for the monitoring of hydrological processes and applications [Petropoulos et al., 2015].

Many studies have recently focused on exploring the complementarity and interchangeability between different EO data and modelling approaches aiming at offering a potential solution to decompose (or disaggregate) passive microwave SSM estimates to higher spatial or temporal resolutions, particularly based on the synergy with visible, infrared and thermal information [Merlin et al., 2010; Piles et al. 2011;2014; Sánchez-Ruiz et al., 2014]. In this respect, these methods exploit the relationships that exist between a satellite-derived estimate of surface temperature (LST), vegetation index (VI), and soil moisture [see review by Petropoulos et al., 2009]. One of the key advantages of using the LST/VI method is that complex parameterisation of aerodynamic and surface resistances for water and heat transfer can be avoided; meanwhile, the so-called "triangle" feature space is able to capture the availability of SSM over heterogeneous surfaces allowing for the variability of SSM to be measureable over large areas [Petropoulos et al., 2009]. Furthermore, these approaches have shown they can potentially provide an easier transformation between instantaneous and daytime averaged fluxes, highlighting the potential application of these methods for the operational estimation of SSM, which has been underlined by a number of investigators [Petropoulos and Carlson, 2010; Piles et al., 2014; Fontanelli et al., 2012]. Indeed, variants of this method have already been subject of research investigations aiming at developing operational estimates of SSM from the National Polar-orbiting Operational Environmental Satellite System (NPOESS) and its use has already been demonstrated using 1 km AVHRR and 25 km SSM/I data (Chauhan et al., 2003). Another variant has been used to improve the spatial resolution of SSM estimates from SMOS globally distributed products using MODIS LST/VI [Piles et al., 2011; 2014].

The SMOS downscaling algorithm first presented in Piles et al. [2011] utilises a combination of SMOS brightness temperatures with higher resolution VIS/IR data from MODIS via an extension of the "triangle" technique to obtain operational estimates of SSM at 1 km spatial resolution that are at present available for the Iberian Peninsula [Piles et al, 2014]. These maps have routinely been used in forest fire prevention services since 2012 [Piles et al., 2013, Chaparro et al., 2015a], and have been shown to be useful in a variety of other applications, such as Gross Primary Productivity estimation [Sánchez-Ruiz et al., 2015], and forest die-off prediction models [Chaparro et al., 2015b]. This synergistic concept has also been applied to downscale SMOS/MODIS to 500 m using a SWIR-based VI [Sánchez-Ruiz et al., 2014], and to retrieve very high spatial resolution soil moisture from hyperspectral optical, thermal and microwave L-band airborne observations [Sánchez et al., 2014]. Although this technique is able to provide SSM estimates at 1 km spatial resolution, its temporal resolution depends on the presence of clouds, which mask MODIS observations, and is therefore limited in its temporal capability. Polar-orbiting satellites, such as NASA's Terra/Aqua, provide a limited number of MODIS images of a given site on a daily basis (up to a maximum of 4 per day). Geostationary meteorological satellites, in turn, provide data every 15', greatly increasing the possibilities of having clear-sky conditions at a given site on a daily basis [Zhang et al., 2014].

In the present study, a methodology for deriving SSM maps from EO data at previously unattained spatio-temporal resolutions is proposed. The approach is based on the synergistic use of EO data from the MIRAS-SMOS and SEVIRI-MSG instruments and it allows to: (1) enhance the spatial resolution of the SMOS SSM estimates to 3 km spatial resolution, and, (2) provide a temporal extrapolation of the instantaneous fine-scale downscaled SSM estimates acquired every 15 minutes from SMOS between 6

a.m. to 6 p.m. to a "daytime SSM" estimate. The proposed algorithm has been applied to SMOS/SEVIRI observations acquired over the Iberian Peninsula and Southern France covering a complete calendar year (2011). Validation of the derived SSM maps has been undertaken against collocated *in-situ* measurements from REMEDHUS (Spain), Vas (Spain) and SMOSMANIA (France) permanent soil moisture measurement networks, utilising ground measurements acquired from a total of 40 stations. Those were selected carefully to represent a variety of climatic, topographic and environmental conditions and allow for the inclusion of contrasting conditions.

2. DATASETS DESCRIPTION & PRE-PROCESSING (IN-SITU, SATELLITE, ANCILLARY)

2.1 ISMN soil moisture: REMEDHUS, SMOSMANIA and VAS

In-situ soil moisture was obtained from REMEDHUS, SMOSMANIA and VAS *in-situ* monitoring networks through the International Soil Moisture Network (ISMN, Dorigo et al., 2011). The locations of the *in situ* networks considered for this study are presented in Fig. 1.

<Insert Figure 1 here>

REMEDHUS is composed of 23 automated soil moisture monitoring stations located in an area of 1300 km^2 in a semi-arid sector of the Duero basin in Spain (Figure 1) (41.1º to 41.5º N, and 5.1º to 5.7º W). Each station within the network is equipped with capacitance probes (Hydra Probes of Stevens Water Monitoring System, Inc.) installed horizontally at a depth of 5 cm, integrating measurements over a depth of 0-5 cm with a reported accuracy of 0.003 $m^3\ m^{-3}$. This dataset provides a continuous measurement of soil moisture each hour. The homogeneity of the area makes it ideal for the validation of all kinds of soil moisture products as shown in the use of this network in a number of validation exercises. Data from the REMEDHUS network have also been used previously to study the spatial and temporal dynamics of soil moisture [Martínez-Fernandez and Ceballos, 2003] and for satellite product validation [Ceballos et al., 2005; Liu et al., 2011; Parinussa et al., 2011]. The land use is mainly agricultural, consisting primarily of rainfed cereals grown in winter and spring (78%), irrigated crops in summer (5%), and perennial vineyards (3%) and forest-pasture areas (13%). This area is nearly flat (less than 12% slope) and ranges from 700 to 900 m. a. s. l. The regional climate is continental semi-arid Mediterranean with an average annual precipitation of 385 mm and a mean temperature of 12ºC [Sánchez et al., 2012]. More details on the equipment installed at the stations itself can be found in Sanchez et al. [2012]. For the time period included in this study (i.e. year 2011), data from 19 REMEDHUS stations were available (out of the 23).

SMOSMANIA is a long-term data acquisition network based on the existing automatic weather station network of Meteo-France (RADOME - Réseau d'Acquisition de Données d'Observations Météorologiques Etendu). Twenty one existing stations of RADOME in southwestern France were chosen for inclusion in the SMOSMANIA project. The network consists of a 400 km transect based on 21 automatic weather stations (the average distance between two neighbouring stations is approximately 40 km) forming a Mediterranean-Atlantic gradient equipped with 4 capacitance probes (ThetaProbe ML2X of Delta-T Devices) at each site measuring soil moisture at four different depths (5, 10, 20, and 30 cm). Stations have obtained data since January 2007 with a 12 minute time step. The vegetation cover at those sites consists of natural fallow, harvested once or twice a year, where the area is relatively flat (except for 3 sites with an altitude above 500 ma.s.l.) [Calvet et al., 2007; Albergel et al., 2008]. Data from the top soil 5 cm over the year 2011 were used in this study. Measurements taken by this network have been

extensively used for validating various satellite-based soil moisture products [Albergel et al., 2009, 2010; Li et al., 2010; Brocca et al., 2011; Liu et al., 2011; Parinussa et al., 2011]. Data from 19 SMOSMANIA stations were used.

The Valencia Anchor Station (VAS) network is comprised of 3 stations established in 2001 by The University of Valencia as a robust automatic meteorological station located towards the North-West part of the Utiel-Requena Plateau in the Valencia region, close to the town of Caudete de las Fuentes (39°3 N, 1°1W) at about 80 km from the city of Valencia [López-Baeza et al., 2003]. The network represents a reasonably homogeneous and mostly flat area of about 50×50 km^2. The main land cover type is vineyards, about 56%, followed by trees, shrubs, forest, industrial and urban. Beside the vineyard growing season, the area remains mostly under bare soil conditions. The climate oscillates between semi-arid and dry-sub-humid with annual mean temperatures variations from 12 ◦C to 14.2◦C and annual precipitation variations between 396 mm to 451 mm [Juglea et al., 2010]. Two VAS stations soil moisture measurements acquired with capacitance probes (Hydra Probes and Theta Probes ML2X) from the top soil 5 cm over the year 2011 were used in this study.

As already noted above, the half-hourly SSM observations acquired at the surface layer (0-5 cm) for the year 2011 were obtained for the above (40 in total) ISMN sites. For each day, the *in situ* soil moisture at SMOS morning overpass time (6 a.m.) was extracted. Subsequently, the *in situ* half-hourly observations registered from 6 a.m. to 6 p.m. were averaged to match SMOS/SEVIRI daytime average soil moisture estimates. It should be noted that if any hourly granules for the period between 6 a.m. to 6 p.m. were missing or contained an error value, these days were excluded from any further analysis.

2.2 SMOS L3 soil moisture

The ESA SMOS mission was launched on 2 November 2009 as the second Earth Explorer Opportunity mission to be developed as part of ESA's Living Planet Programme. This polar orbiting satellite operates in a sun-synchronous orbit at a mean altitude of 758 km and an inclination of 98.44°, with a spatial resolution of 40-50 km operating through a dusk-down orbit with a 3 day revisit at the equator [Kerr et al., 2010]. The Microwave Imaging Radiometer with Aperture Synthesis (MIRAS) is the main instrument onboard the SMOS platform which records emitted energy from the Earth's surface in the microwave L-band (1.4 GHz) with the aim of providing soil moisture estimates at accuracies better than 0.04 m^3 m^{-3}. The SMOS BEC L3 daily global soil moisture product v.1 from the Barcelona Expert Center (BEC) was used in this study. It is available in netCDF format through the CP34-BEC web service (http://cp34-bec.cmima.csic.es/), and is obtained through quality filtering and binning the ESA's SMUDP2 product (v5.51) to a regular grid; the original L2 estimates with negative soil moisture values and/or DQX values greater than 0.07 are discarded, and a weighted average is applied to bin the data to a 25 km EASE-ML regular grid [see further details in González-Zamora et al, 2015]. This SMOS product includes geophysical parameters, a theoretical estimate of their accuracy, and a set of product flags and descriptors. A comprehensive evaluation of this product using two complementary small-scale and large-scale *in-situ* networks and a surface water balance model was performed in González-Zamora et al. [2015]. Results showed that SMOS BEC L3 soil moisture estimates were consistent with SMOS L2 and *in-situ* measurements in the time series comparisons, with Pearson's correlation coefficients (R) and an Agreement Index (AI) higher than 0.8 for the total average and the land-use averages and higher than 0.85 for the soil-texture averages.

2.3 SEVIRI LST, FVC

SEVIRI is a geostationary orbit optical imaging radiometer which serves as the main payload on-board the MSG satellite. This is a co-funded space mission between the European Space Agency (ESA) and EUMETSAT. SEVIRI has 12 spectral channels, consisting of three Visible and Near-InfraRed (VNIR) channels (centered at 0.6, 0.8 and 1.6 μm), eight InfraRed (IR) channels (centred at 3.9, 6.2, 7.3, 8.7, 9.7, 10.8, 12.0 and 13.4 μm) and one visible broadband channel (at 0.5–0.9 μm) called the High Resolution Visible channel (HRV). The satellite provides image data at 3 km spatial resolution at the sub-satellite point (nadir) for standard channels, and down to 1 km for the HRV channel, providing permanent visible and infrared imaging of the Earth's disc, over 4 specific geographical regions (Europe, Africa - North_Africa and South_Africa- and South America), with a baseline repeat cycle of 15 minutes [Aminou 2002; Sobrino and Romaguera, 2004]. A series of operational products from SEVIRI are provided by EUMETSAT such as Land Surface Temperature (LST) and Fractional Vegetation Cover (FVC). Those are distributed by the Satellite Application Facility (SAF) on Land Surface Analysis (LSA) (http://landsaf.meteo.pt/).

The retrieval of SEVIRI LST is based on clear-sky measurements from the MSG system in the thermal infrared window (IR 10.8 and 12.0 μm MSG/SEVIRI channels) and has been generated on an operational basis since February 2005 for the European region and since July 2005 for the whole Meteosat disk. The main algorithm for LST estimation is based on a Generalized Split Window (GSW) that uses the difference between two adjacent window channels to correct the atmospheric absorption [Caselles et al., 1997]. Theoretically, LST values can be determined 96 times per day from MSG but in practice fewer observations are available due to cloud cover. For this study, the SEVIRI LST product was downloaded for the Euro region of the Meteosat disk for the year 2011. For each time-slot and geographical region, the LST field and respective Quality Control (QC) data was acquired in Hierarchical Data Format (HDF5) and HDF5 file attributes [LSA-SAF 2015].

The SEVIRI FVC product is generated daily at the full spatial resolution of the MSG/SEVIRI instrument (3 km). The product is computed using as input the three short-wave channels (VIS 0.6μm, NIR 0.8μm, SWIR 1.6μm) and a parametric BRDF (Bi-directional Reflectance Distribution Function) model [Roujean et al. 1992]. In the product, fractional vegetation cover amount is expressed as percentage (%), ranging from 0 to 100%, corrected from uncertainty derived of the view/sun angles and also the anisotropy effects of surface reflectance in the SEVIRI image. The FVC product includes routine quality check and error estimates. Herein, the SEVIRI FVC product was downloaded for the Euro region of the Meteosat disk for the year 2011. For each day and geographical region, the FVC product, its error estimate and the processing flag were acquired in Hierarchical Data Format (HDF5) file attributes [LSA-SAF 2015].

All the acquired SEVIRI datasets were reprojected from Normalized Geostationary Projection (NGP) to a regular latitude/longitude grid and tailored from the full disk image to the study region (34º-45ºN, 11ºW-5ºE). Subsequently, each image was subsetted to cover only the countries on which the experimental sites were located. All these steps were implemented using Matlab routines available.

3. SPATIO-TEMPORAL DOWNSCALING

3.1 Physical Properties of the LST/VI Scatterplot Domain in respect to SSM

The LST/VI methods, including the “triangle” inversion modelling technique, have their basis in the relationships obtained between SSM and satellite-derived Vegetation Index (VI), such as the FVC, and LST are plotted in a two-dimensional scatterplot. Provided that cloudy and water pixels have been

masked out and that there is a full variability of FVC cover in the acquired satellite data, in such a scatterplot, a triangular/trapezoidal-shape has been shown to emerge. This is the result of the low sensitivity of LST to variations of SSM over vegetated areas, but its increased sensitivity (and thus greater spatial variation) over areas of bare soil. In this triangular/trapezoidal space, the dry (warm) and wet (cold) edges provide important boundary conditions for the contextual LST-VI (or FVC) relationship. The theoretical "dry edge" is the triangular space boundary representing maximum soil water-limiting conditions for the plant canopy, characterised by maximum water stress derived from limiting conditions of soil moisture or evapotranspiration. In contrast, the "wet edge" is the LST-VI space boundary for pixels representative of maximum soil wetness conditions or surfaces with limited or no water stress. Based on these specific boundary conditions, SSM can be derived for any given satellite pixel and a range of techniques have been proposed to do so exploiting a wide range of appropriate EO data [for a recent review see Petropoulos et al., 2009].

3.2 Algorithm for SSM estimation at high spatio-temporal resolution using SMOS and SEVIRI data

In this study, the potential use of the SEVIRI LST/VI sensitivity to estimate soil moisture variations within a coarse-scale SMOS pixel is evaluated. To do so, an algorithm for soil moisture estimation at MSG high spatio-temporal resolution (3 km, 15 minutes), exploiting the synergies between SMOS and SEVIRI observations has been developed. It builds upon the algorithm used for the operational SMOS/MODIS 1 km soil moisture product available at BEC. Details concerning the implementation of this technique are available in Piles et al. [2014]. The proposed technique consists of a semi-empirical model— a regression formula— that links SMOS- and SEVIRI-derived information to SSM as follows:

$$SSM = a_0 + a_1 \cdot LST + a_2 \cdot FVC + \sum_{i=1}^{3} a_{3i} \cdot T_{BH\theta i} + \sum_{i=1}^{3} a_{4i} \cdot T_{BV\theta i}, \quad (1)$$

where *LST* is SEVIRI normalized LST, *FVC* is SEVIRI Fractional Vegetation Cover, and $T_{BH\theta i}$ and $T_{BV\theta i}$ are normalized horizontal and vertically polarized brightness temperatures, respectively, at incidence angles θ_i of 32.5º, 42.5º and 52.5º. Normalization is performed between the minimum and maximum values registered within the study area per overpass/acquisition.

Parameters in the model are represented in the two spatial scales under consideration (i.e. SMOS 25 km and SEVIRI 3 km): *LST* and *FVC* are aggregated to 25 km and $T_{BH\theta i}$ and $T_{BV\theta i}$ are resampled at 3 km. The model is first applied at low resolution for all image pixels using SMOS L3 as soil moisture reference at coarse-scale to determine the coefficients. Subsequently, the model is applied at high resolution using the obtained coefficients to estimate the fine-scale SMOS-derived soil moisture.

SMOS/SEVIRI instantaneous SSM estimates can be temporally averaged to achieve higher coverage (in case the presence of clouds masks SEVIRI data) and representativeness (up to 48 estimates per pixel can be obtained for SMOS ascending and SEVIRI daytime, with a total of 96 per day). Also, an estimate of the daytime average SSM value is considered of more practical use in many applications in comparison to the instantaneous estimate [Barrett and Petropoulos, 2013]. Different combinations of available SMOS and MODIS images were composited into a temporally averaged downscaled soil moisture estimate in a previous study, as a first step towards increasing the spatio-temporal coverage in SSM data [Merlin et al., 2012]. It is hypothesized the availability of high frequency SEVIRI observations will allow for improved coverage and robust daily mean soil moisture estimates, with respect to the use of polar orbiting satellites. Also, the high temporal frequency of the estimates paves the way for the development of gap-filling approaches for complete coverage [Dumedah et al., 2014; Turlapaty et al, 2012; Wang et al., 2012]. In this regard, both the instantaneous and the temporally-averaged SSM estimates could

prove useful depending on the application. Hence, in this study we use SMOS ascending (6 a.m.) and SEVIRI daytime (6 a.m. to 6 p.m.) observations from year 2011 to generate a data set of SSM instantaneous estimates at the time of SMOS overpass (hereafter L4 instant) and a data set of SSM average values from 6 a.m. to 6 p.m. (hereafter L4 daytime). We evaluate the performance of the two retrievals separately from comparison with *in-situ* data. Also, the number of observations per pixel used to obtain the daytime averages is registered to evaluate the minimum number of SEVIRI snapshots required to obtain a representative daytime estimate.

4. STATISTICAL ANALYSIS

Three time-series of SSM derived from the EO data were compared to *in-situ* data from the 40 ISMN stations: 1) SMOS L3 SSM at 6 a.m. and 25 km spatial resolution, 2) SMOS/SEVIRI SSM at 6 a.m. at 3 km spatial resolution (L4 instant), and 3) SMOS/SEVIRI SSM average from 6 a.m. to 6 p.m. observations at 3 km spatial resolution (L4 daytime).

The spatial resolution enhancement is evaluated with SMOS L3 and SMOS/SEVIRI L4 instant data sets (Section 5.1). The agreement of the two data sets against the collocated *in-situ* data was evaluated based on direct point-by-point comparisons at every *in situ* station (n=40). In addition, a dedicated analysis to evaluate the efficiency, precision, and accuracy of the downscaling approach has been performed.

The spatio-temporal resolution enhancement is evaluated with the L4 daytime product (Section 5.2); for every *in situ* station, all averaged measurements acquired from 6 a.m. to 6 p.m. are compared with their corresponding L4 daytime, i.e. the average of the available SMOS/SEVIRI instantaneous SSM estimates from 6 a.m. to 6 p.m. An additional analysis was performed using the L4 daytime data set to evaluate the minimum number of SEVIRI observations per pixel (i.e. cloud-free snapshots) required to ensure the representativeness of the daytime estimate. The accuracy of L4 daytime SSM series was analysed separately at every *in situ* station for days with different percentage coverage: 0-24%, 25-49%, 50-74% and 75-100%.

An analysis of the three SSM time series at the network scale (Section 5.3) is also performed to ensure that the agreement of the fine-scale soil moisture is not due to a representative issue (i.e. an *in situ* probe being more representative of the 1 km surrounding it, than of the 25 km surrounding it). When network averages are used, all the 3 km and 25 km pixels over *in situ* stations are averaged.

Eight statistical performance assessment metrics were used to evaluate the agreement between satellite and *in situ* measurements. These included the Root Mean Square Difference (RMSD), the unbiased or centered RMSD (cRMSD), the Pearson's Correlation Coefficient (R), the bias (*in-situ* minus estimated), the scatter or standard deviation, (Entekhabi et al., 2010). The p-value at 95% and 99% confidence level was used to determine the series with non-significant correlation. These statistical metrics have also been widely used in similar validation experiments carried out previously (e.g. Falge et al. 2005; Giertz et al., 2006; Marshall et al., 2013). In addition, the slope a and intercept b of a robust regression are computed using iterative re-weighted least squares (Street et al., 1988), which is less influenced by the outliers than the ordinary least squares fit. Three dedicated metrics (G_EFFI, G_PREC, G_ACCU) to evaluate the performance of the downscaling algorithm have also been computed (Merlin et al., 2015). G_EFFI characterizes the efficiency of the disaggregation method; if the downscaling approach is efficient, the slope between satellite retrievals and *in situ* soil moisture should increase and be closer to one in the disaggregation case, relative to the non-disaggregation case (G_EFFI > 1). The precision of a downscaling algorithm can be seen as the degree to which repeated application under unchanged

conditions shows the same downscaled value; the gain in precision can be estimated as the gain in R (G_PREC > 1). Finally, the gain in accuracy in the downscaling algorithm can be seen as the improvement in the bias obtained with *in situ* data (G_ACCU > 1). Table 1 summarizes the statistical measures implemented in this study to evaluate the agreement between satellite and *in situ* measurements and the performance of the downscaling approach

<Insert Table 1 here>

5. RESULTS

Two sample L4 instant and L4 daytime SSM maps are shown for a dry day (July 31st 2011) and a wet day (December 27th 2011) over the central part of the Duero basin, including the REMEDHUS network (Figure 2). For the dry period (Figure 2, top), the L4 maps clearly show higher soil moisture content near the main rivers. This pattern reflects the irrigated plots close to the rivers (see also Figure 1). These areas are typically well watered during the summer, when the growing cycle of the irrigated plots (corn, sugarbeet) takes place. Also, the wettest areas in this period are found in the south, coinciding with the forested areas of the Sistema Central range (see the location map in Figure 1). This effect is reinforced in the wet period (Figure 2, bottom), where this wet pattern is extended and amplified. Significant differences can be seen between the two products during the wet period. The higher soil moisture content obtained in L4 daytime most probably integrates rain events in the area during the time lapse between 6 a.m. to 6 p.m., which are not captured by the L4 instant. This hypothesis was supported as well by the records of precipitation at this day from two rain gauge stations of the Spanish Meteorological Agency located in the southern area of the map, which registered 0.2 mm at 11 a.m.. The spatial and temporal patterns of SSM are consistent for the two products, but a slightly higher dynamic range can be detected in the L4 instant (Figure 2 a). These qualitative differences are quantified in the statistical analysis hereafter.

<Insert Fig. 2 here>

5.1 Spatial resolution enhancement: SMOS/SEVIRI SSM instantaneous measurements

The comparison of SMOS L3, SMOS/SEVIRI L4 instant and collocated *in-situ* measurements at 6 a.m. from three representative stations of low water content (07-REMEDHUS), high water content (Narbonne-SMOSMANIA), and intermediate water content (Melbex1-VAS) for year 2011 are shown in Fig. 3. The evolution of soil moisture trends reveals that both SMOS L3 and L4 instant slightly underestimate the SSM content in the three stations. Coarse and fine scale SSM estimates agree well with *in situ* measurements and follow closely the dry-downs and wetting-up events. The scatter plots of L3 and L4 instant *vs. in situ* SSM (Figure 3, right), in turn, show that there is a good correspondence between satellite and ground-based SSM estimates, with SMOS L3 providing to some extent a better agreement in terms of slope (closer to the 1:1 line) and the L4 instant showing an improved correlation in Narbonne. This underlines and quantifies what has already been shown with the temporal plots: the L4 instant product preserves the quality of the SMOS L3 product whilst improving its spatial representation through integration of SEVIRI LST/FVC information.

<Insert Fig. 3 here>

The detailed statistical results from comparison with the 40 ISMN stations are displayed in Tables 2 and 3 for SMOS L3 AND SMOS/SEVIRI L4 instant, respectively. Comparing the two tables, it can be observed

that L3 and L4 instant have a similar performance in terms of R. The L4 product appears to have a generally slightly smaller correlation than L3, and only in 13 stations R is improved from L3 to L4. However, the most remarkable improvement is evidenced in the statistical metrics of cRMSD, with the latter being decreased dramatically in the L4 at 33 stations out of 40. Results in terms of RMSD for L3 and L4 instant are comparable.

The bias of L3 is mostly positive (dry bias), suggesting an underestimation of the remotely sensed product in comparison to the in-situ (reference dataset). Notably, eleven out of 19 stations in REMEDHUS, 16 out of 19 in SMOSMANIA and the two VAS stations show a dry bias. This SMOS L3 dry bias is consistent with recent and on-going calibration studies on SMOS coarse-resolution data at a variety of sites, which indicates a general underestimation of SMOS retrievals with respect to 0-5 cm soil moisture measurement [Al Bitar et al., 2012; Gherboudj et al, 2012; González-Zamora 2015]. The dry bias in the L3 product was generally stressed in SMOSMANIA (the network with the highest soil moisture content) but, when the series were unbiased (cRMSD), the performance of the L3 product was similar in the two networks.

The improvement of slope, correlation and bias of the L4 instant product with respect to the SMOS L3 is quantified through the G_EFFI, G_PREC and G_ACC metrics (in Table 3). These gains indicate what stations result in an improvement of the associated statistics after the downscaling (positive gain sign, indicated in bold in Table 3), and to what extent (the larger the gain value, the higher the degree of improvement). A positive gain means that the downscaling improves the spatial representativeness of SSM data at the validation scale, relative to the low-resolution data (Merlin et al., 2015). Taking these metrics as a reference, 11 out of 40 stations present an improvement in efficiency (slope), 14 show an improvement in precision (R) and 21 reflect an improvement in accuracy (bias), confirming the improvement found for the errors in Table 3. Hence, more than half of the stations present improved statistics at the fine-scale.

The improvement of the cRMSD/bias of the L4 with respect to L3 should be particularly highlighted. Also, some stations in REMEDHUS and SMOSMANIA had an unreasonable bias (bigger than 0.15 $m^3 m^{-3}$) in the two products, probably related with irrigation supply at these particular plots (Sánchez et al., 2012; Liu et al, 2014).

<Insert Tables 2, 3 here>

In order to assess the downscaling performance separately from the SMOS/SEVIRI synergy at high (3 km) and low (25 km) resolution, a comparison between 25 km resolution aggregated L4 SMOS/SEVIRI soil moisture and the original 25 km resolution L3 SMOS soil moisture was made through G_EFFI, G_ACCU and G_PREC (Table 4). First, it is noticeable that the L4 aggregated product behaves similarly to the high resolution L4 in terms of R (similar to L3) and root-mean-squared errors (smaller than L3). Second, the gain analysis shows even better results than the L4 high resolution gains (Table 3), i.e., 11 out of 40 stations improved the efficiency, 15 showed an improvement in precision and 25 reflect an improvement in accuracy. Thus, it can be concluded that the gain results of the L3 *vs.* L4 instant are comparable to those of the L3 *vs.* L4 aggregated, even slightly better in the latter. This indicates that the proposed downscaling scheme not only provides a better representativeness of the resulting product owing its better resolution, but also allows for a qualitatively improvement due to the inclusion of SEVIRI data.

<Insert Table 4 here>

5.2 Spatio-temporal downscaling: SMOS/SEVIRI SSM daytime composites

The comparison of instantaneous L4 daytime and collocated *in situ* measurements from three representative stations of low water content (07-REMEDHUS), high water content (Narbonne-SMOSMANIA), and intermediate water content (Melbex1-VAS) are shown in Fig. 4. From the time-evolution plots, it can be seen that L4 daytime follows the range and temporal dynamics of the *in situ* daytime measurements at station 07, and shows a general underestimation at Narbonne and Melbex 1, in line with results for L3 and L4 instant on Fig. 3. The slope obtained for the L4 daytime estimates (Fig. 4, right) are closer to the 1:1 line than with the L4 instant (Fig. 3, right).

<Insert Fig. 4 here>

The statistical results from comparison with the 40 ISMN stations are displayed in Table 5 for SMOS/SEVIRI L4 daytime. Note that the daytime average is computed with *in situ* data using all measurements acquired from 6 a.m. to 6 p.m. but with the satellite data only with the cloud-free snapshots during this time lapse. Hence, this analysis is focused on assessing how representative a daytime composite is of the mean soil moisture conditions.

Comparing the two L4 estimates (Tables 3 and 5), it is clear that L4 instant showed better correlations than L4 daytime in 31 stations. Regarding the errors and bias statistics, a slightly smaller cRMSD is obtained for the L4 instant ($0.033\ m^3\ m^{-3} < cRMSD < 0.137\ m^3\ m^{-3}$) than for L4 daytime ($0.044\ m^3\ m^{-3} < cRMSD < 0.146\ m^3\ m^{-3}$). As expected, the accuracy of the instantaneous product is higher that that of the time-integrated, since the representativeness of L4 daytime highly depends on the cloud-free snapshots that can contribute to the daytime average.

<Insert Table 5 here>

The number of SSM instantaneous estimates per 3 km pixel used to obtain the L4 daytime product was registered as ancillary information with the retrievals. This information has been used to evaluate the minimum number of observations required to obtain a representative daytime estimate. To do so, the L4 daytime product was divided into four thresholds dependent on the percentage of SEVIRI snapshots with data: 0-24%, 25-49%, 50-74%, 75-100%. Subsequently, R and cRMSD statistics were computed for each station and threshold. Results for the 9 stations that have significant correlation at a 95% in the four-percentage coverage considered are shown in Fig. 6. As a general trend, it is seen that higher R are obtained for coverages greater than 25% and lower cRMSD are obtained for coverages greater than 50%. These results indicate that the high temporal resolution of SEVIRI not only allows increasing the possibility of cloud-free conditions for a given region, but also provides more accurate temporally-averaged SSM estimates. The 0-24% coverage was significant in 14 out of the 40 ISMN stations, whereas the other percentages were significant in 26-30 stations. As expected, the stations with at least a 25% daytime SEVIRI coverage provide a representative averaged SSM estimate in a higher number of locations.

<Instert Fig. 5 here>

These results suggest that the information on sub-hourly scale variability in LST from SEVIRI (LST being the only parameter in Eq. 1 that varies from 6 a.m. to 6 p.m.) has an important impact on the estimated SSM. Indeed, the correlation between SEVIRI land surface temperature and soil moisture is expected to vary at the hourly scale during the day (Pablos et al., 2014). Further work of interest would be directed towards the validation of the methodology at the time step of SEVIRI and to the analysis of the SSM- LST relationship dependence on season and time of the day.

5.3 Overview of SSM time series at the network scale

The comparison of network averages is summarised in Fig. 6 and Table 6. Scatter plots are shown for instantaneous (left column) and daytime (right column) remotely sensed *vs*. *in situ* measurements. These scatter plots follow the same pattern that that of the individual stations, i.e., a slight underestimation of the observed soil moisture and a good fit between series, slightly worse for the L4 daytime estimations. Again, since SMOSMANIA is the wettest area, its slope is around 0.5, and its bias and cRMSD is the higher of the three networks (Table 6). Results for network averages support that SSM spatial patterns are captured at the 3 km scale, with L4 instant providing improved R and cRMSD over REMEDHUS and VAS networks. Statistical results for REMEDHUS (first row) and VAS (third row) are comparable to the ones shown in Fig. 3 and 4 for stations O7 and Melbex 1, respectively. This can be explained by the fact that these two networks cover an area of approximately one SMOS pixel and can be considered relatively homogeneous. The SMOSMANIA network covers a wider area of ~40 SMOS pixels, and results shown for Narbonne station in Figs. 4 and 5 differ to the ones obtained for the network average in Fig. 6. In particular, cRMSD are higher and the slopes of the linear regression are lower for the network average than for the individual stations. This fact can also explain the better fit of REMEDHUS and VAS than SMOSMANIA for all products.

< Insert Fig. 6 here >

It is important to note that different sensors in each network (ThetaProbe ML2X from Delta-T Devices in SMOSMANIA and VAS *vs.* Hydraprobes from Stevens Inc. for REMEDHUS and VAS) may lead to a certain bias in the comparisons presented. Even though both have the same principle measurement (capacitance probes), and that site-specific calibration curves were developed using *in situ* gravimetric soil samples in each network, their comparative accuracy and performance in different field scenarios may need to be investigated when used altogether (Albergel et al. 2012). This could particularly explain the lower performance of both L4 and L3 over SMOSMANIA stations, together with topographic and possible irrigation effects.

One can argue that the better agreement of SMOS/SEVIRI L4 than SMOS L3 to *in situ* shown in sections 5.1 and 5.2 were due to high resolution SSM estimates being more representative of a SSM point measurement than coarse resolution estimates. Indeed, the representativeness of the *in situ* measurements appears to have a clear impact in the validation, especially over highly heterogeneous sites. Nonetheless, as has been shown in this section, the results obtained at individual stations are also confirmed using network averages.

6. DISCUSSION AND CONCLUSIONS

This study has explored the potential for obtaining high spatio-temporal soil moisture mapping from the combination of SMOS and SEVIRI remotely sensed observations. A synergistic technique has been presented that allows estimating instantaneous soil moisture every 15' at 3 km spatial resolution from spaceborne data. The instantaneous SMOS/SEVIRI SSM estimates are of special interest for hydrological modelling and applications where information on SSM at high spatio-temporal resolution may be used to initialise and update forecasts, storm water management, flood or hydrological models. Also, evidently, they have the potential to be temporally averaged if the purpose is to achieve higher coverage (in case the presence of clouds masks SEVIRI data) and representativeness (up to 48 estimates per pixel can be obtained for SMOS ascending and SEVIRI daytime). In this study, the instantaneous SSM

estimates acquired at the time of SMOS morning overpass (6 a.m., L4 instant) and the SSM daytime average (computed with observations available from 6 a.m. to 6 p.m., L4 daytime) have been validated using a year of SMOS and SEVIRI observations over the Iberian Peninsula and Northern France. A comprehensive validation has been undertaken using collocated *in situ* measurements from three permanent soil moisture networks: REMEDHUS, VAS and SMOSMANIA acquired over a full year (2011). The performances of the downscaling approach and the disaggregated soil moisture maps were evaluated separately using a series of statistical metrics.

Results from statistical analysis at individual stations showed that combining SMOS/SEVIRI into L4 instant SSM estimates preserves the quality of the SMOS L3 product whilst improving its spatial representation. L3 generally underestimated the ground-based measurements of soil moisture (Table 2), as previously observed with the L2-derived L3 products (González-Zamora et al. 2015) and L2 itself (Sánchez et al., 2012; dall'Amico et al., 2012). This bias is improved in the L4 product, which shows a significantly lower cRMSD at 33 stations (Tables 2 and 3). The two products have a similar performance in terms of R (slightly lower for L4 instant) and RMSD.

Specific performance metrics were used to assess the gain in efficiency, precision and accuracy after the downscaling at high (3km) and low (25 km aggregated) resolutions (Merlin et al., 2015). Results for L4 instant show that 11 out of 40 stations present an improvement in efficiency (slope), 14 present an improvement in precision (R) and 21 present an improvement in accuracy (bias). The results obtained for L4 instant aggregated are comparable, even slightly better (15 stations with improved R and 25 with improved bias). Hence, taking these metrics as reference, the downscaling has improved the spatial representativeness of SSM data from 25 to 3 km in more than half of the stations. These results suggest that the synergistic SMOS/SEVIRI retrieval approach proposed herein provides a pathway for an improved SSM characterization, in comparison to using SMOS data alone.

This work explored as well the feasibility of soil moisture spatio-temporal downscaling. To do so, SSM was estimated at the temporal resolution of the MSG geostationary platform (15') and used to compose a daytime average with increased coverage in case of clouds. Results from comparison with individual stations showed that L4 daytime provides a representative estimate of *in-situ* measurements (Fig. 6, Table 5), with coverage higher than 25% leading to higher R and coverage higher than 50% lead to lower cRMSD (Fig. 6). As expected, L4 instant provides more accurate SSM estimates that L4 daytime when a minimum coverage is not imposed. Still, the higher performance of L4 instant versus L4 daytime can also be influenced by the fact that at 6 a.m. the weather conditions are very stable (lack of insolation nor evaporation/evapotranspiration). Indeed, the correlation between *in-situ* soil moisture at 6 a.m. and the daily average *in-situ* in the studied networks is very high (R=0.96 for both REMEDHUS and VAS and R=0.91 for SMOSMANIA). Hence, in no-rain conditions the L4 instant product at 6 a.m. is representative of average daily conditions. Further research should be directed towards the analysis of the SSM-LST relationship dependence on time of the day and its impact in the disaggregated SSM estimates.

The number of observations available for the L4 daytime series is notably higher (more than 100 in most cases) than for the L4 instant (between ~40 and 90). This is (one of) the main advantages of using SEVIRI VIS/IR information to enhance passive microwave data versus the use of polar orbiting satellites (e.g. MODIS). Results from Fig. 3 and Table 3 showed that L4 instant obtained from SMOS/SEVIRI is comparable to the SSM estimates obtained from SMOS/MODIS (Piles et al, 2014; Sánchez-Ruiz et al., 2014). Hence, by combining SMOS with a geostationary satellite it was shown that instantaneous SSM estimates of similar quality than when using a polar satellite can be provided. More importantly, it was shown that an averaged SSM value with higher coverage can be obtained and that the SSM evolution

every 15'can be potentially estimated. Further research may be directed towards exploring the SSM instantaneous measurements obtained at the sub-daily scale with the aim of providing robust composites and also at studying the added value of the high frequency observations in highly dynamic SSM contexts such as an irrigated field or intense rain events.

The inter-comparison of the three remotely sensed SSM series (L3, L4 instant and L4 daytime) at the network scale was also presented in this study. The results obtained at individual stations for each product are confirmed using network averages, supporting that spatial patterns are captured at the 3 km scale (Fig. 6, Table 6). Regarding the comparison of L3 and L4 instant, result for network averages over REMEDHUS and VAS are consistent to those obtained for individual stations, with L4 instant providing slightly higher R and lower cRMSD. In contrast, results for SMOSMANIA reveal a lower R and higher bias and mean squared errors for L4 in regards to L3. This result suggests that the spatial variability of soil moisture fields across SMOSMANIA is perhaps not captured by simple linear spatial average of point-based measurements (Crow et al., 2002). It is important to note that whereas REMEDHUS and VAS stations are distributed within the area of a SMOS pixel, SMOSMANIA provides sparse ground-based measurements covering an area of approximately 40 SMOS pixels. This different network topology may also explain the degraded accuracy of the estimates obtained in SMOSMANIA in all the statistical analyses with respect to REMEDHUS and VAS.

The analysis of the daily spatial correlation between SMOS-derived and *in-situ* SSM estimates to show spatial coherency of remotely sensed maps is debatable due to both the mismatch of point *vs.* footprint scales and the difficulty of having a sufficient number of estimates at a temporal snapshot to obtain significant results (González-Zamora et al, 2015). A land surface model may be useful to bridge this gap and further analyze the spatial variability of remotely sensed SSM estimates. An in-depth comparison of the SSM spatial structures that are resolved by SMOS and by a land surface model was presented in (Polcher et al, 2015). Results showed a good temporal correlation between modeled and remotely sensed SSM but a poor match of spatial co-variances, probably due to disagreements found in the effective inertia of the soil moisture reservoir (SMOS observing a shallower and faster soil moisture reservoir than the model). In this regard, the proposed method could provide an interesting data set of remotely sensed SSM estimates at high spatial resolution but also at the sub-daily scale to offer more insight in the comparisons of remotely sensed, *in-situ*, and modeled SSM. A continuous effort in this direction is needed to support the use of remote sensing SSM in data assimilation schemes for improved weather forecasts and climate predictions (Seneviratne et al., 2010).

Variability in atmospheric conditions and land surface characteristics impacts the variability in soil moisture at different spatial scales. Previous experimental studies have reported two separate scales of variation of soil moisture, one smaller scale, dominated by land surface variations, and a second larger scale, influenced by meteorological processes (Entin et al., 2000, Brocca et al., 2007, Lakhankar et al., 2010). In this regard, the proposed model captures the spatial variability in land surface conditions at the higher spatial resolution of the SEVIRI data (i.e. Ts, FVC), and the influence of atmospheric conditions, determined by precipitation and evaporation patterns at the SMOS larger scale (i.e. brightness temperatures). The downscaling technique can therefore be potentially implemented at any area size covered under the field of view of the required input satellite data. However, the impact of non-linear interactions between the canopy, the soil and the atmospheric circulation, caused by changing atmospheric or landscape conditions and not captured by the proposed semi-empirical model may certainly place a limit to the extension of the area used to apply the methodology. Further investigation into the relationships of optical and microwave observations and derived parameters at different spatial scales could help resolving this question.

Our study contributes towards on-going efforts aimed at developing a global operational SSM product applicable at the spatio-temporal resolution required in a wide spectrum of application and research studies. The proposed method offers a very promising potential to allow for the first time monitoring of the Earth's SSM at previously unattained spatial and temporal resolutions, and consequently transform the way we utilize EO data to obtain a better understanding of Earth's water and energy cycles. The latter is today one of the key research priorities to be addressed by the global scientific community. Last but not least, the EO-based SSM products developed and presented in this study open potentially a new trail for the development of applications using EO data at previously unattained spatio-temporal resolutions, greatly increasing the scientific and societal return of the economic investment in space missions.

ACKNOWLEDGMENTS

This research was supported by the Spanish Ministry of Science and Innovations and the European Regional Development Fund (ERDF) through the MIDAS-7 project (AYA2012-39356-C05) and by the European Space Agency's Support to Science Element (STSE) PROgRESSIon" project. Partial funding was also received from the BBVA Foundation. Gareth's Ireland's participation was funded by the EU Marie Curie TRANSFORM-EO project. Finally, authors wish to thank to the anonymous reviewers for their valuable and useful suggestions that clearly improved the paper.

REFERENCES

1. Al Bitar, A., Leroux, D., Kerr, Y. H., Merlin, O., Richaume, P., Sahoo, A., & Wood, E. F. (2012). Evaluation of SMOS soil moisture products over continental US using the SCAN/SNOTEL network. Geoscience and Remote Sensing, IEEE Transactions on, 50(5), 1572-1586.
2. Albergel, C., de Rosnay, P., Gruhier, C., Muñoz-Sabater, J., Hasenauer, S., Isaksen, L., Kerr, Y., & Wagner, W. (2012). Evaluation of remotely sensed and modelled soil moisture products using global ground-based in situ observations. Remote Sensing of Environment, 118 215-226
3. Albergel, C., Rüdiger, C., Carrer, D., Calvet, J. C., Fritz, N., Naeimi, V., ... & Hasenauer, S. (2009). An evaluation of ASCAT surface soil moisture products with in-situ observations in Southwestern France. Hydrology and Earth System Sciences, 13(2), 115-124.
4. Albergel, C., Rüdiger, C., Pellarin, T., Calvet, J. -C., Fritz, N., Froissard, F., et al. (2008). From near-surface to root-zone soil moisture using an exponential filter: An assessment of the method based on in situ observations and model simulations. Hydrology and Earth System Sciences, 12, 1323–1337, doi:10.5194/hess-12-1323-2008.
5. Aminou, D. M. A. (2002). MSG's SEVIRI instrument. ESA Bulletin(0376-4265), (111), 15-17.
6. Barrett, B. & G.P. Petropoulos (2013): Satellite Remote Sensing of Surface Soil Moisture. Chapter 4, pages 85-120, in "Remote Sensing of Energy Fluxes and Soil Moisture Content ", by G.P. Petropoulos, Taylor Francis, ISBN: 978-1-4665-0578-0.
7. Brocca, L., R. Morbidelli, F. Melone, T. Moramarco (2007). Soil moisture spatial variability in experimental areas of central Italy, Journal of Hydrology, Vol. 333, 356-373.
8. Brocca, L., Hasenauer, S., Lacava, T., Melone, F., Moramarco, T., Wagner, W., ... & Bittelli, M. (2011). Soil moisture estimation through ASCAT and AMSR-E sensors: An intercomparison and validation study across Europe. Remote Sensing of Environment, 115(12), 3390-3408.
9. Calvet, J.-C.; Fritz, N.; Froissard, F.; Suquia, D.; Petitpa, A.; Piguet, B., (2007) In situ soil moisture observations for the CAL/VAL of SMOS: the SMOSMANIA network, Geoscience and Remote

Sensing Symposium, 2007. IGARSS 2007. IEEE International , vol., no., pp.1196,1199, doi: 10.1109/IGARSS.2007.4423019.
10. Caselles V., E. Valor, C. Coll and E. Rubio, (1997). Thermal band selection for the PRISM instrument 1. Analysis of emissivity-temperature separation algorithms, J. Geophs. Res., 102, D10, 11145-11164.
11. Ceballos, A., Scipal, K., Wagner, W., & Martinez-Fernandez, J. (2005). Validation of ERS scatterometer-derived soil moisture data in the central part of the Duero Basin, Spain. Hydrological Processes, 19(8), 1549-1566.
12. Chaparro, D; M. Vall-llossera, M. Piles, A. Camps, C. Rüdiger (2015a), Low Soil Moisture and High Temperatures as indicators for Forest Fire Ocurrence and Extent across the Iberian Peninsula, Proc. IEEE International Geoscience and Remote Sensing Symposium, 3325-3328.
13. Chaparro, D; Vayreda, J; Vall-llossera, M; Banqué, M; Piles, M; Camps, A; Martínez-Vilalta, J, (2015b) Regional patterns of forest decline are associated with climatic anomalies and remotely sensed soil moisture, Ecological Applications, in review.
14. Chauhan, N. S., Miller, S., & Ardanuy, P. (2003). Spaceborne soil moisture estimation at high resolution: a microwave-optical/IR synergistic approach. International Journal of Remote Sensing, 24(22), 4599-4622.
15. Crow, W. T., A. A. Berg, M. H. Cosh, A. Loew, B. P. Mohanty, R. Panciera, P. deRosnay, D. Ryu, and J. P. Walker (2012), Upscaling sparse ground-based soil moisture observations for the validation of coarse-resolution satellite soil moisture products, Rev. Geophys., 50, RG2002
16. dall'Amico, J.T.; Schlenz, F.; Loew, A.; Mauser, W. (2012). First results of SMOS soil moisture validation in the Upper Danube Catchment. IEEE Transactions on Geoscience and Remote Sensing, 50, 1507-1516
17. Dorigo, W.A., Wagner, W., Hohensinn, R., Hahn, S., Paulik, C., Xaver, A., Gruber, A., Drusch, M., Mecklenburg, S., van Oevelen, P., Robock, A., and Jackson, T., Jackson, T. (2011), "The International Soil Moisture Network: A data hosting facility for global in situ soil moisture measurements", Hydrology and Earth System Sciences 15 (5), pp. 1675-1698.
18. Dumedah, G.; Jeffrey P. Walker, Li Chik, Assessing artificial neural networks and statistical methods for infilling missing soil moisture records (2014), Journal of Hydrology, Volume 515, Pages 330-344, ISSN 0022-1694
19. Entekhabi, D., Reichle, R. H., Koster, R. D., & Crow, W. T. (2010). Performance metrics for soil moisture retrievals and application requirements.Journal of Hydrometeorology, *11*(3), 832-840.
20. Entin, J. K., Robock, A., Vinnikov, K. Y., Hollinger, S. E., Liu, S., & Namkhai, A. (2000). Temporal and spatial scales of observed soil moisture variations in the extratropics. Journal of Geophysical Research: Atmospheres (1984-2012), 105, 11865-11877.
21. Falge, E., Reth, S., Brüggemann, N., Butterbach-Bahl, K., Goldberg, V., Oltchev, A. and Bernhofer, C. (2005). Comparison of surface energy exchange models with eddy flux data in forest and grassland ecosystems of Germany. Ecol. Model., 188, 174-216.
22. FAO (2015). Chapter 4 - Remote Sensing as a Data Source; Fishieries and Aquaculture Department, Food and Agriculture Organization of the United Nations [online]. Available at: http://www.fao.org/docrep/003/t0446e/t0446e04.htm [Accessed 19 June 2015].
23. Gherboudj, I., Magagi, R., Goïta, K., Berg, A., Toth, B., & Walker, A. (2012). Validation of SMOS data over agricultural and boreal forest areas in Canada. Geoscience and Remote Sensing, IEEE Transactions on, 50(5), 1623-1635.
24. Giertz, S., Diekkrüger, B. and Steup, G. (2006) Physically-based modelling of hydrological processes in a tropical headwater catchment (West Africa)–process representation and multi-criteria validation. Hydrol. Earth Syst. Sc., 10, 829-847.

25. GOSIC, Facilitating Access to Global Observing Systems Data and Information (2015). Global Observing Systems Information Center, [onine] Available at: http://www.gosic.org/ [Accessed 19 June 2015].
26. González-Zamora, A; N. Sánchez, J. Martínez-Fernández, A. Gumuzzio, M. Piles, E. Olmedo (2015) Long-term SMOS soil moisture products: a comprehensive evaluation across scales and methods in the Duero Basin (Spain), Journal of Physics and Chemistry of the Earth, vol. 83-84, 123-136.
27. Juglea, S., Kerr, Y., Mialon, A., Wigneron, J. P., Lopez-Baeza, E., Cano, A., ... & Delwart, S. (2010). Modelling soil moisture at SMOS scale by use of a SVAT model over the Valencia Anchor Station. Hydrology and Earth System Sciences, 14(5), 831-846.
28. Kerr, Y; P. Waldteufel, J.-P. Wigneron, S. Delwart, F. Cabot, J. Boutin, M.-J. Escorihuela, J. Font, N. Reul, C. Gruhier, S. Juglea, M. R.Drinkwater, A. Hahne, M. Martin-Neira, and S. Mecklenburg, (2010) The SMOS mission: New Tool for Monitoring Key Elements of the Global Water Cycle, Proc. IEEE, vol. 98, pp. 666–687.
29. Lakhankar, T., Jones, A.S., Combs, C.L., Sengupta, M., Vonder Haar, T.H., Khanbilvardi, R. (2010) Analysis of Large Scale Spatial Variability of Soil Moisture Using a Geostatistical Method. *Sensors*, Vol. 10, 913-932.
30. Li, B., Rodell, M., Zaitchik, B. F., Reichle, R. H., Koster, R. D., & van Dam, T. M. (2012). Assimilation of GRACE terrestrial water storage into a land surface model: Evaluation and potential value for drought monitoring in western and central Europe. Journal of Hydrology, 446, 103-115.
31. Liu, Y. Y., Parinussa, R. M., Dorigo, W. A., De Jeu, R. A. M., Wagner, W., Van Dijk, A. I. J. M., ... & Evans, J. P. (2011). Developing an improved soil moisture dataset by blending passive and active microwave satellite-based retrievals. Hydrology and Earth System Sciences, 15(2), 425-436.
32. López-Baeza, E., Velázquez, A., Antolín, C., Bodas, A., Gimeno, J. F., Saleh, K., ... & Sánchez, M. A. (2003). The Valencia Anchor Station, a Cal/Val Reference Area for Largescale Low Spatial Resolution Remote Sensing Missions. In Proc. 3rd International Conference on Experiences with Automatic Weather Stations (pp. 19-21).
33. LSA – SAF (2015), Land Surface Temperature (15 mins), Land Surface Analysis Satellite Applications Facility [online]. Available at: http://landsaf.meteo.pt/algorithms.jsp?seltab=0&starttab=0 [Accessed 19 June 2015].
34. Marshall, M., Tu, K., Funk, C., Michaelsen, J., Williams, P., Williams, C. and Kutsch, W., (2013) Improving operational land surface model canopy evapotranspiration in Africa using a direct remote sensing approach. Hydrol. Earth Syst. Sc., 17, 1079-1091.
35. Martínez-Fernández, J., & Ceballos, A. (2003). Temporal stability of soil moisture in a large-field experiment in Spain. Soil Science Society of America Journal, 67(6), 1647-1656.
36. Merlin, O., A. A. Bitar, J. Walker, and Y. Kerr, (2010) "An improved algorithm for disaggregating microwave-derived soil moisture based on red, near-infrared and thermal-infrared data," Remote Sens. Environ., vol. 114, pp. 2305–2316.
37. Merlin, O., C. Rudiger, A. Al Bitar, P. Richaume, J. P. Walker, and Y. H. Kerr (2012), Disaggregation of SMOS soil moisture in Southeastern Australia, IEEE Trans. Geosci. Remote Sens., 50 (5), 1557-1571.
38. North, M. R., Petropoulos, G.P., Rentall, D.V., Ireland, G.I. & J.P. McCalmont (2015): Evaluating the capability of a land biosphere model in simulating land surface processes: results from different European Ecosystems. DOI : doi:10.5194/esdd-6-217-2015 Earth Surface Dynamics Discussions.
39. Ochsner, T. E., Cosh, M. H., Cuenca, R. H., Dorigo, W. A., Draper, C. S., Hagimoto, Y., ... & Zreda, M. (2013). State of the art in large-scale soil moisture monitoring. Soil Science Society of America Journal, *77*(6), 1888-1919.

40. Pablos, M.; Piles, M.; Sanchez, N.; Gonzalez-Gambau, V.; Vall-llossera, M.; Camps, A.; Martinez-Fernandez, J. (2014) A sensitivity study of land surface temperature to soil moisture using in-situ and spaceborne observations, Proc. IEEE Int. Geosci. Remote Sens. Symp , pp. 3267-3269.
41. Panciera, R., Walker, J. P., Jackson, T. J., Gray, D., Tanase, M., Ryu, D., ... & Hacker, J. M. (2014). The soil moisture active passive experiments (SMAPEx): Toward soil moisture retrieval from the SMAP mission. Geoscience and Remote Sensing, IEEE Transactions *on*, *52*(1), 490-507.
42. Parinussa, R. M., Holmes, T. R. H., Yilmaz, M. T., & Crow, W. T. (2011). The impact of land surface temperature on soil moisture anomaly detection from passive microwave observations. Hydrology and Earth System Sciences, 15(10), 3135-3151.
43. Petropoulos, G. P., Ireland, G., & Barrett, B. (2015). Surface soil moisture retrievals from remote sensing: Current status, products & future trends. Physics and Chemistry of the Earth, Parts A/B/C.
44. Petropoulos, G., Carlson, T. N., Wooster, M. J., & Islam, S. (2009). A review of Ts/VI remote sensing based methods for the retrieval of land surface energy fluxes and soil surface moisture. Progress in Physical Geography, *33*(2), 224-250.
45. Petropoulos, G.P., Ireland, G., Srivastava, P.K., & Ioannou-Katidis, P. (2014). An appraisal of the accuracy of operational soil moisture estimates from SMOS MIRAS using validated in situ observations acquired in a Mediterranean environment. International Journal of Remote Sensing, 35, 5239-5250.
46. Piles, M., Sánchez, N., Vall-llossera, M., Camps, A., Martínez-Fernández, J., Martínez, J., & González-Gambau, V. (2014). A dowscaling approach for SMOS land observations: long-term evaluation of high resolution soil moisture maps over the Iberian Peninsula. IEEE Journal of Selected Topics in Applied Earth Observations and Remote Sensing, 7, 3845-3857.
47. Piles, M, A. Camps, M. Vall-llossera, A. Monerris, M. Talone (2011). Downscaling SMOS-derived soil moisture using MODIS visible/infrared data. IEEE Transactions on Geoscience and Remote Sensing. 49, pp. 3156 – 3166, doi: 10.1109/TGRS.2011.2120615.
48. Piles, M, M Vall-llossera, A. Camps, N. Sánchez, J. Martínez-Fernández, J. Martínez, V. González-Gambau. (2013), On the synergy of SMOS and Terra/Aqua MODIS: high resolution soil moisture maps in near real-time, Proc. IEEE International Geoscience and Remote Sensing Symposium, pp. 3423 - 3426. 2013.
49. Polcher, Jan, M. Piles, E. Gelati, A. Barella-Ortiz, M. Tello (2015). Comparing surface-soil moisture from the SMOS mission and the ORCHIDEE land-surface model over the Iberian Peninsula, Remote Sensing of the Environment, in press.
50. Riveros-Iregui, D. A., McGlynn, B. L., Emanuel, R. E., & Epstein, H. E. (2012). Complex terrain leads to bidirectional responses of soil respiration to interannual water availability. Global Change Biology, *18*(2), 749-756.
51. Roujean, J. L. (1992). for the Correction of Remote Sensing Data. Journal of geophysical research, 97(D18), 20-455.
52. Sánchez, N., Martinez-Fernandez, J., Scaini, A., Perez-Gutierrez, C., (2012a). Validation of the SMOS L2 Soil Moisture Data in the REMEDHUS Network (Spain). IEEE Transactions on Geoscience and Remote Sensing, 50: 1602-1611.
53. Sánchez-Ruiz, S., Piles, M., Sánchez, N., Martínez-Fernández, J., Vall-llossera, M., Camps, A., (2014). Combining SMOS with visible and near/shortwave/thermal infrared satellite data for high resolution soil moisture estimates. Journal of Hydrology(0).
54. Sánchez-Ruiz, S, Moreno, A, Martínez, B, Piles, M, Maselli, F, Carrara, A, Gilabert, M.A (2015). Impact of water stress on GPP estimation from remote sensing data in Mediterranean ecosystems, Proc. Recent Advances on Quantitative Remote Sensing, in press.

55. Seneviratne, S.I., T. Corti, E.L. Davin, M. Hirschi, E.B. Jaeger, I. Lehner, B. Orlowsky, A.J. Teuling, (2010). Investigating soil moisture-climate interactions in a changing climate: A review. Earth-Science Reviews, 99, 3-4, 125-161.
56. Shen, C., Niu, J., & Fang, K. (2014). Quantifying the effects of data integration algorithms on the outcomes of a subsurface–land surface processes model. Environmental Modelling & Software, 59, 146-161.
57. Shen, C., Niu, J., & Phanikumar, M. S. (2013). Evaluating controls on coupled hydrologic and vegetation dynamics in a humid continental climate watershed using a subsurface-land surface processes model. Water Resources Research,*49*(5), 2552-2572.
58. Sobrino, J. A., & Romaguera, M. (2004). Land surface temperature retrieval from MSG1-SEVIRI data. Remote Sensing of Environment, 92(2), 247-254.
59. Statement Of Guidance For Hydrology And Water Resources, (2014). World Meteorological Organisation [pdf] Available at: https://www.wmo.int/pages/prog/www/OSY/SOG/SOG-Hydrology.pdf [Accessed: 10th July 20-15]
60. Street O. J., Raymond J. Carroll and David Ruppert, (1988). A Note on Computing Robust Regression Estimates Via Iteratively Reweighted Least Squares. The American Statistician. Vol. 42, No. 2,pp. 152-154
61. Turlapaty, A.C., Younan, N.H., Anantharaj, V.G., (2011). Interpolation of Missing Values in AMSR-E Soil Moisture Data Using Modified SSA," *Geoscience and Remote Sensing Letters, IEEE* , vol.8, no.2, pp.322,325, doi: 10.1109/LGRS.2010.2071852.
62. Wagner, W., Hahn, S., Kidd, R., Melzer, T., Bartalis, Z., Hasenauer, S., ... & Rubel, F. (2013). The ASCAT soil moisture product: A review of its specifications, validation results, and emerging applications. Meteorologische Zeitschrift, 22(1), 5-33.
63. Wang, G., D. Garcia, Y. Liu, R. de Jeu, A. J. Dolman, A three-dimensional gap filling method for large geophysical datasets: Application to global satellite soil moisture observations, (2012). Environmental Modelling & Software, Volume 30, Pages 139-142, ISSN 1364-8152, http://dx.doi.org/10.1016/j.envsoft.2011.10.015.
64. Wood, E. F., Roundy, J. K., Troy, T. J., Van Beek, L. P. H., Bierkens, M. F., Blyth, E., ... & Whitehead, P. (2011). Hyperresolution global land surface modeling: Meeting a grand challenge for monitoring Earth's terrestrial water.Water Resources Research, *47*(5).
65. Zhang, D., Tang, R., Zhao, W., Tang, B., Wu, H., Shao, K., & Li, Z. L. (2014). Surface soil water content estimation from thermal remote sensing based on the temporal variation of land surface temperature. Remote Sensing, *6*(4), 3170-3187.
66. Zhao, W., & Li, A. (2013). A downscaling method for improving the spatial resolution of AMSR-E derived soil moisture product based on MSG-SEVIRI data. Remote Sensing, 5(12), 6790-6811.

List of Figures:

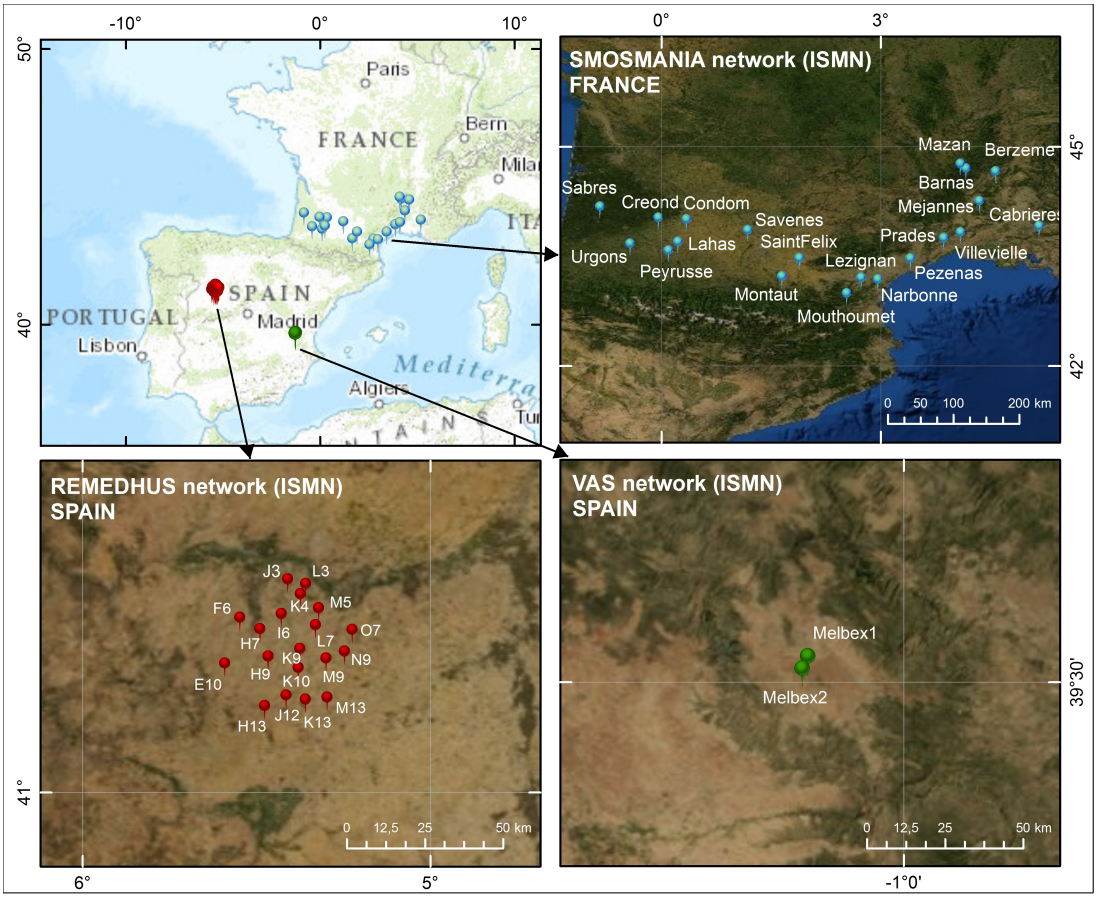

Fig.1. Location of the 40 International Soil Moisture Network (ISMN) validation sites used in the study. Top left: location of the sites within Europe (image acquired from Google Maps). Top right: location of the SMOSMANIA sites in southern France. Bottom left: location of the REMEDHUS sites in the Duero Basin in Spain. Bottom right: location of the Valencia Anchor Station (VAS) sites in southern Spain.

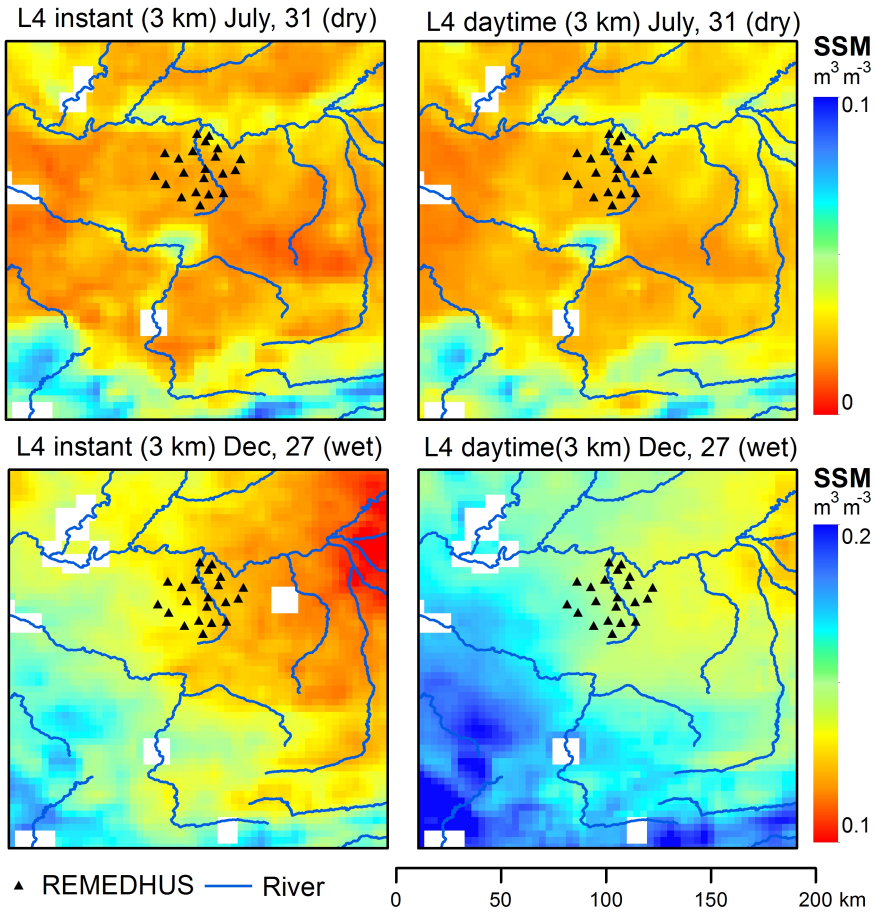

Fig.2. SSM distribution over the REMEDHUS network for the SMOS/SEVIRI L4 Instantaneous (left) and the SMOS/SEVIRI L4 Daytime Average (right) obtained for a dry day on July 31st 2011 (top) and a wet day on December 27th 2011 (bottom).

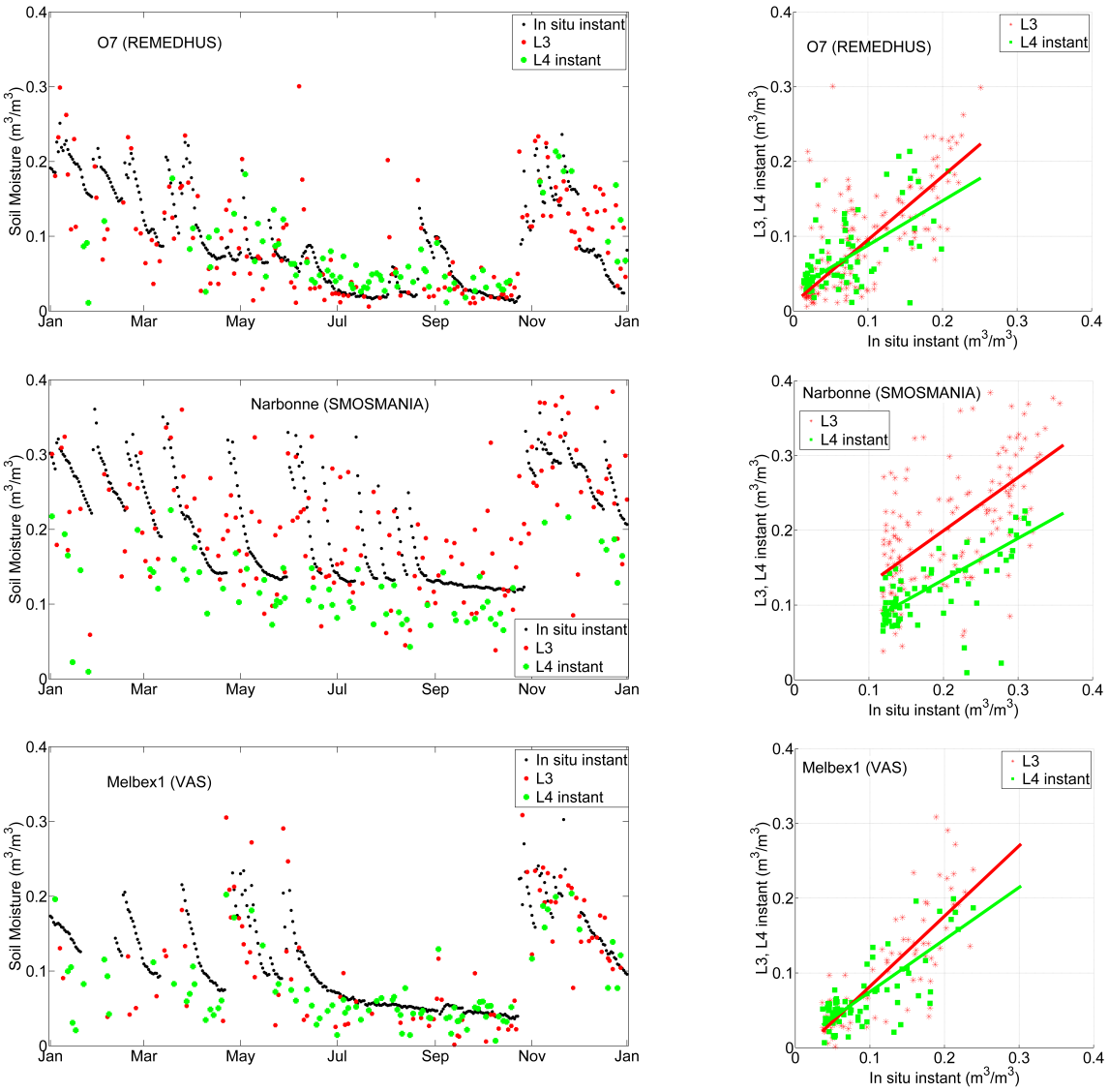

Fig. 3. Evolution of soil moisture trends (left column) and scatter plots (right column) for L4 instant, L3 and collocated in-situ measurements for year 2011 at representative stations: 07 (first row), Narbonne (second row) and Melbex1 (third row).

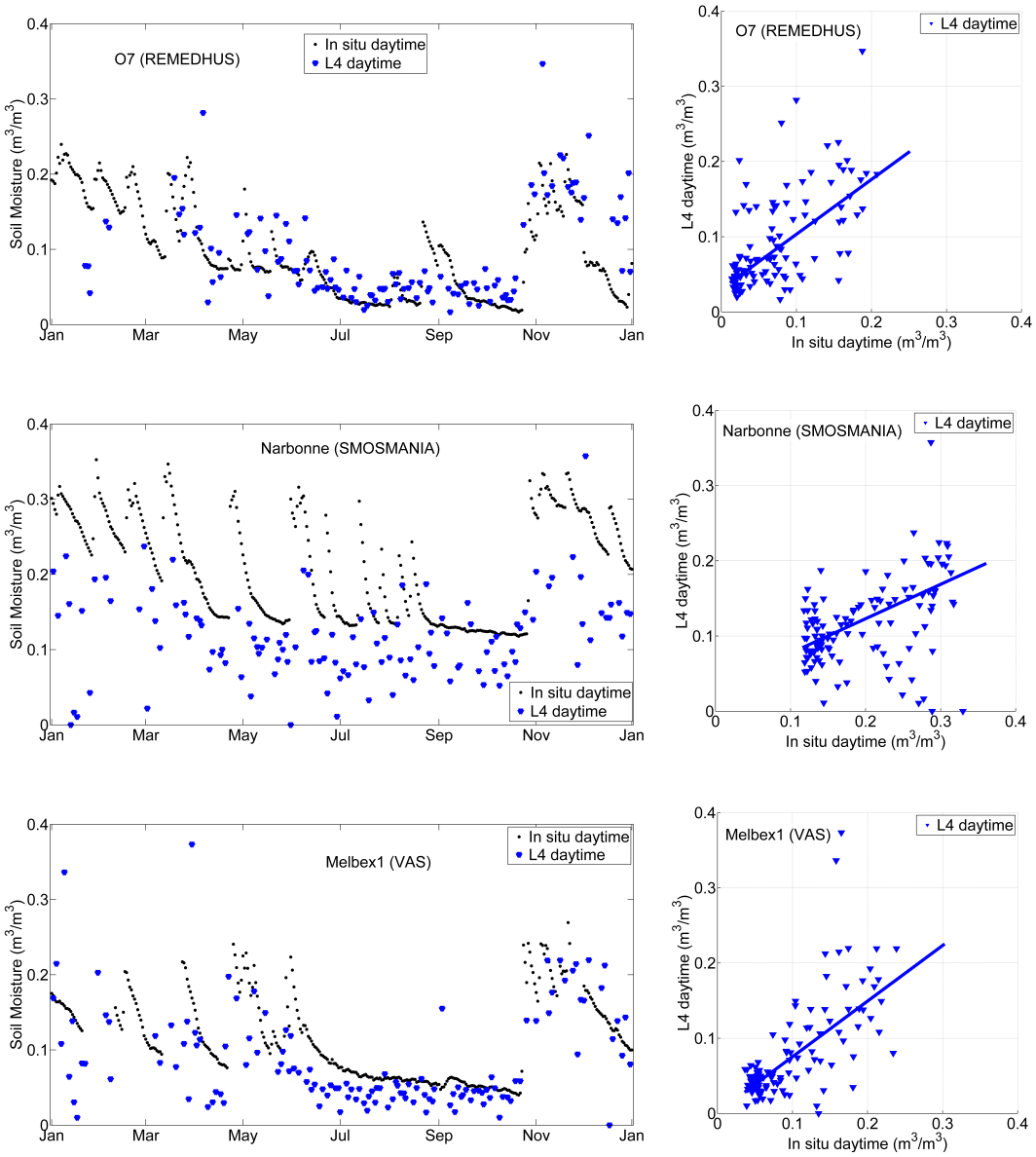

Fig. 4. Evolution of soil moisture trends (left column) and scatter plots (right column) for L4 daytime and collocated in-situ measurements for year 2011 at representative stations: 07 (first row), Narbonne (second row) and Melbex1 (third row).

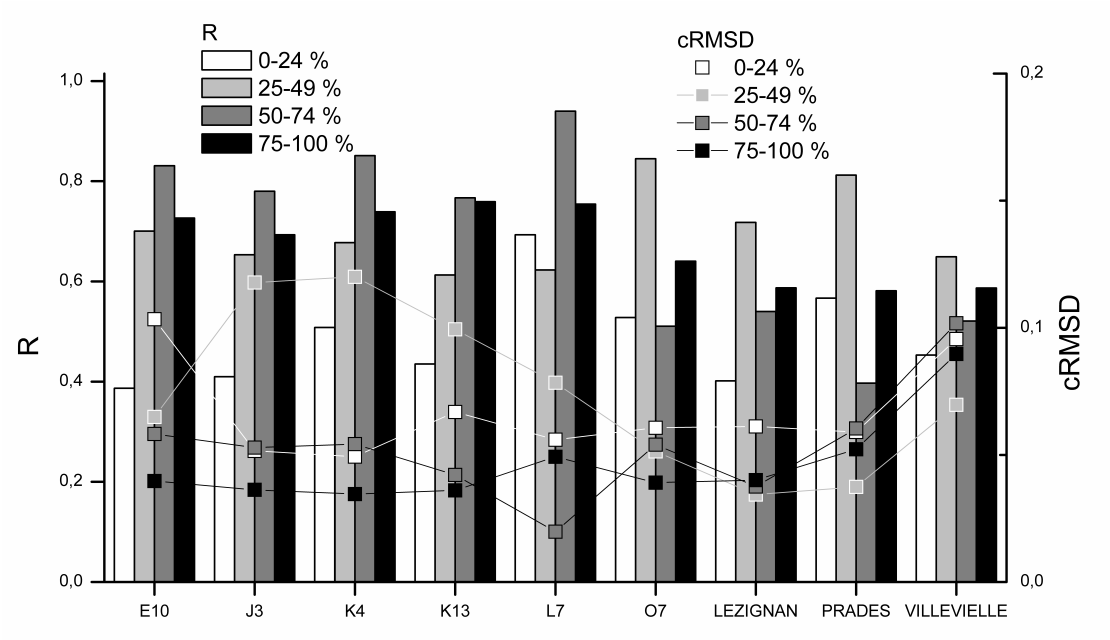

Fig. 5. R and cRMSD of the L4 daytime product divided into thresholds dependent on the percentage of SEVIRI overpasses (0-24%, 25-49%, 50-74%, 75-100%) available for each day of analysis. Results are shown only for the stations that have significant correlation at a 95% in the four percentages coverage considered.

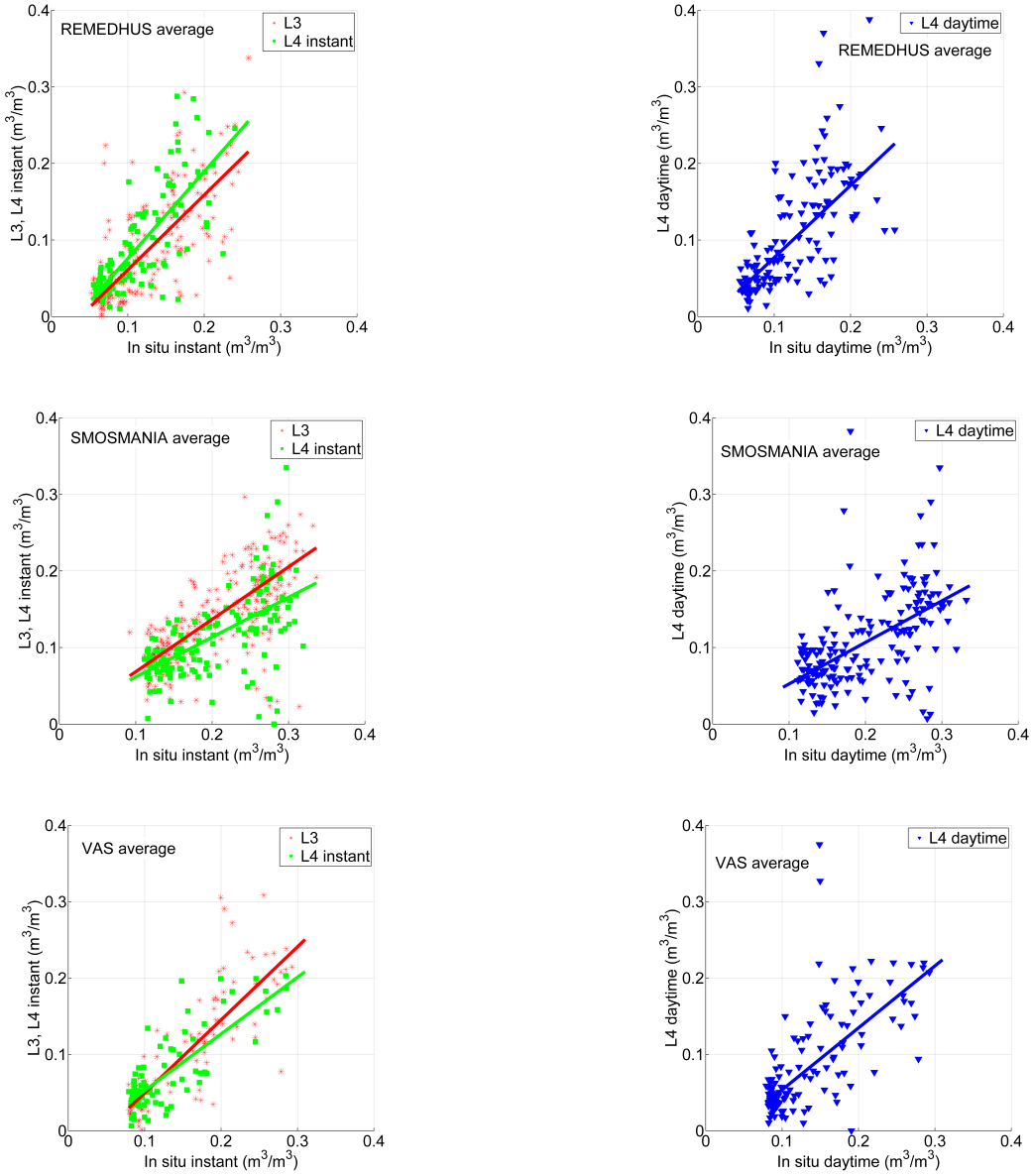

Fig. 6. Scatter plots of satellite *vs.* ground-based measurements of instantaneous (left column) and daytime (right column) soil moisture measurements. Results are shown for year 2011 for the average of each network: REMEDHUS (first row), SMOSMANIA (second row), and VAS (third row).

Table 1. Statistical measures computed to evaluate the agreement between satellite and *in situ* soil moisture measurements and the performance of the downscaling approach. $E[\cdot]$ is the expectation operator, σ_{sat} is the standard deviation of satellite measurements θ_{sat}, $\sigma_{in\text{-}situ}$ is the standard deviation of in situ measurements $\theta_{in\text{-}situ}$, a is the slope of the linear regression between satellite and in situ soil moisture. Subscripts L3 and L4 indicate statistics associated to SMOS L3 and SMOS/SEVIRI L4 products.

Name	Description	Mathematical Definition
bias/*B*	Mean bias	$bias = E\left[\theta_{sat}\right] - E\left[\theta_{in-situ}\right]$
R	Linear time series correlation	$R = \frac{E\left[(\theta_{sat} - E[\theta_{sat}])(\theta_{in-situ} - E[\theta_{in-situ}])\right]}{\sigma_{sat}\sigma_{in-situ}}$
RMSD	Root Mean Square Difference	$RMSD = \sqrt{E\left[(\theta_{sat} - \theta_{in-situ})^2\right]} = \sqrt{\sigma_{sat}^2 + \sigma_{in-situ}^2 - 2 \cdot r \cdot \sigma_{sat} \cdot \sigma_{in-situ} + B^2}$
cRMSD	Unbiased or Centred RMSD	$cRMSD = \sqrt{\sigma_{sat}^2 + \sigma_{in-situ}^2 - 2 \cdot r \cdot \sigma_{sat} \cdot \sigma_{in-situ}}$
G_{EFFI}	Dissagregation efficiency gain	$G_{EFFI} = \frac{\lvert 1 - a_{L3} \rvert - \lvert 1 - a_{L4} \rvert}{\lvert 1 - a_{L3} \rvert + \lvert 1 - a_{L4} \rvert}$
G_{PREC}	Dissagregation precision gain	$G_{PREC} = \frac{\lvert 1 - R_{L3} \rvert - \lvert 1 - R_{L4} \rvert}{\lvert 1 - R_{L3} \rvert + \lvert 1 - R_{L4} \rvert}$
G_{ACCU}	Dissagregation accuracy gain	$G_{ACCU} = \frac{\lvert B_{L3} \rvert - \lvert B_{L4} \rvert}{\lvert B_{L3} \rvert + \lvert B_{L4} \rvert}$

Table 2. Summary of the statistical metrics (R, RMSD, cRMSD, bias, slope *a* and intercept *b* of the linear regression, and number of observations N) for the individual comparisons between the SMOS L3 against concurrent *in situ* observations at each network. Stations with not-significant correlation at 0.05/0.01 confidence level are indicated by */** respectively.

REMEDHUS	R	RMSD	cRMSD	bias	*a*	*b*	N
E10	0,74	0,103	0,055	-0,087	2,045	0,049	124
F6	0,45	0,085	0,074	0,043	0,624	0,002	152
H7	0,63	0,102	0,068	-0,076	4,257	-0,031	146
H9	0,71	0,299	0,167	0,248	0,254	0,010	152
H13	0,78	0,056	0,047	0,031	0,937	-0,026	152
I6	0,71	0,104	0,061	-0,084	3,729	0,030	170
J3	0,71	0,095	0,055	-0,077	2,107	0,045	170
J12	0,74	0,193	0,054	0,185	0,770	-0,124	152
K4	0,77	0,086	0,055	-0,067	2,469	0,008	169
K9	0,40	0,073	0,071	0,019	0,621	0,025	152
K10	0,60	0,088	0,061	-0,064	1,420	0,039	152
K13	0,69	0,126	0,057	0,113	0,814	-0,074	152
L3	0,55	0,062	0,060	-0,017	1,377	-0,018	170
L7	0,66	0,116	0,065	0,097	0,587	-0,023	156
M5	0,50	0,054	0,052	0,013	0,793	0,016	89
M9	0,68	0,102	0,053	0,087	0,785	-0,053	156
M13	0,58	0,213	0,140	0,160	0,224	0,044	124
N9	0,60	0,089	0,060	0,065	0,701	-0,022	156
O7	0,70	0,051	0,051	-0,002	0,850	0,010	156
SMOSMANIA							
Barnas *	0,40	0,143	0,050	0,134	0,244	0,017	22
Berzeme **	0,37	0,114	0,073	0,088	0,301	0,063	44
Condom	0,61	0,176	0,054	0,167	0,707	-0,083	173
Creond	0,66	0,052	0,048	0,020	0,731	0,017	160
Lahas	0,52	0,150	0,081	0,127	0,379	0,049	180
Lezignan	0,76	0,086	0,052	-0,068	1,142	0,057	140
Mazan *	0,34	0,235	0,092	0,216	0,121	0,032	22
Mejannes	0,69	0,123	0,077	0,096	0,438	0,025	114
Montaut	0,68	0,190	0,060	0,180	0,429	-0,008	158
Mouthoumet	0,71	0,074	0,058	0,045	1,176	-0,086	160
Narbonne	0,59	0,072	0,072	0,001	0,712	0,057	156
Peyrusse	0,65	0,117	0,053	0,104	0,659	-0,020	181
Pezenas	0,73	0,079	0,075	-0,025	1,084	0,008	149
Prades	0,69	0,078	0,075	0,021	1,056	-0,036	86
Sabres	-0,29	0,140	0,127	-0,059	-0,229	0,101	82
SaintFelix	0,52	0,106	0,052	0,092	0,854	-0,051	69
Savenes	0,54	0,075	0,070	0,028	0,586	0,046	178
Urgons	0,70	0,206	0,083	0,188	0,347	0,027	172
Villevielle	0,70	0,087	0,079	0,037	0,607	0,037	138
VAS							
Melbex1	0,81	0,057	0,055	0,013	0,940	-0,012	79
Melbex2	0,74	0,101	0,062	0,080	0,865	-0,060	81

Table 3. Summary of the statistical metrics (R, RMSD, cRMSD, bias, slope *a* and intercept *b* of the linear regression, and number of observations N) for the individual comparisons between the SMOS L4 instant and concurrent *in situ* observations at each network. Stations with not-significant correlation at 0.05/0.01 confidence level are indicated by */** respectively. Gains of the downscaling procedure (G_EFFI, G_PREC, G_ACCU) at the 3 km scale with respect to the SMOS L3 product are also shown. Bold indicates positive gain.

REMEDHUS	R	RMSD	cRMSD	bias	*a*	*b*	N	G_EFFI	G_PREC	G_ACC
E10	0,66	0,094	0,050	-0,079	2,53	0,057	66	-0,190	-0,136	**0,050**
F6	0,42	0,074	0,060	0,043	0,62	-0,010	80	-0,004	-0,025	-0,004
H7	0,41	0,079	0,058	-0,054	2,75	-0,007	76	**0,301**	-0,229	**0,170**
H9	0,66	0,229	0,137	0,183	0,25	0,011	84	-0,002	-0,073	**0,151**
H13	0,74	0,048	0,042	0,023	0,76	-0,002	83	-0,574	-0,084	**0,139**
I6	0,73	0,084	0,048	-0,069	3,46	0,033	92	**0,052**	**0,030**	**0,104**
J3	0,76	0,077	0,042	-0,065	2,29	0,045	92	-0,079	**0,098**	**0,090**
J12	0,72	0,185	0,045	0,179	0,63	-0,088	87	-0,232	-0,043	**0,016**
K4	0,70	0,068	0,043	-0,053	1,93	0,022	94	**0,223**	-0,126	**0,117**
K9 *	0,14	0,071	0,062	0,034	0,04	0,056	83	-0,434	-0,181	-0,299
K10	0,53	0,065	0,046	-0,046	1,22	0,034	86	**0,313**	-0,081	**0,161**
K13	0,70	0,120	0,047	0,110	0,53	-0,030	89	-0,428	**0,016**	**0,011**
L3	0,59	0,044	0,043	-0,001	0,87	-0,001	94	**0,496**	**0,050**	**0,881**
L7	0,71	0,093	0,053	0,076	0,47	0,004	87	-0,120	**0,087**	**0,117**
M5 **	0,35	0,057	0,055	0,013	0,53	0,044	37	-0,385	-0,132	-0,006
M9	0,76	0,087	0,038	0,078	0,54	-0,016	77	-0,362	**0,148**	**0,053**
M13	0,60	0,153	0,107	0,109	0,37	0,021	56	**0,110**	**0,024**	**0,188**
N9	0,63	0,077	0,048	0,060	0,50	0,003	83	-0,247	**0,048**	**0,045**
O7	0,63	0,043	0,043	-0,005	0,59	0,028	82	-0,459	-0,096	-0,363
SMOSMANIA										
Barnas	0,58	0,075	0,039	0,064	0,57	0,006	51	**0,283**	**0,174**	**0,353**
Berzeme	0,55	0,087	0,051	0,070	0,56	0,000	21	**0,229**	**0,169**	**0,112**
Condom	0,48	0,201	0,048	0,196	0,49	-0,046	53	-0,262	-0,141	-0,078
Creond	0,45	0,057	0,047	0,031	0,50	0,032	53	-0,298	-0,241	-0,217
Lahas	0,59	0,173	0,078	0,155	0,34	0,021	56	-0,029	**0,082**	-0,098
Lezignan	0,66	0,041	0,033	-0,025	0,72	0,048	53	-0,317	-0,170	**0,465**
Mazan	0,60	0,128	0,095	0,086	0,19	0,062	46	**0,041**	**0,244**	**0,431**
Mejannes	0,58	0,114	0,080	0,081	0,29	0,051	70	-0,114	-0,149	**0,088**
Montaut	0,52	0,186	0,075	0,170	0,25	0,029	49	-0,133	-0,205	**0,030**
Mouthoumet	0,63	0,097	0,044	0,087	0,85	-0,058	61	**0,095**	-0,119	-0,312
Narbonne	0,62	0,081	0,049	0,065	0,55	0,023	69	-0,216	**0,048**	-0,983
Peyrusse	0,54	0,146	0,053	0,136	0,48	-0,011	62	-0,200	-0,129	-0,132
Pezenas	0,72	0,054	0,044	0,032	0,60	0,031	75	-0,651	-0,018	-0,120
Prades	0,59	0,087	0,052	0,070	0,42	0,036	75	-0,823	-0,138	-0,545
Sabres **	0,32	0,116	0,056	-0,101	0,34	0,104	52	**0,304**	**0,311**	-0,262
SaintFelix *	-0,39	0,134	0,060	0,120	-	0,271	20	-0,819	-0,488	-0,132
Savenes	0,50	0,074	0,051	0,053	0,35	0,045	60	-0,220	-0,043	-0,304
Urgons	0,50	0,236	0,101	0,214	0,18	0,043	58	-0,108	-0,247	-0,064
Villevielle	0,67	0,106	0,087	0,061	0,26	0,068	65	-0,305	-0,047	-0,239
VAS										
Melbex1	0,79	0,040	0,033	0,023	0,69	0,005	78	-0,670	-0,044	-0,281
Melbex2	0,70	0,093	0,038	0,085	0,55	-0,023	70	-0,531	-0,076	-0,031

Table 4. Summary of the statistical metrics (R, RMSD, cRMSD, bias, slope *a* and intercept *b* of the linear regression, and number of observations N) for the individual comparisons between the SMOS L4 instant (aggregated into 25 km) against concurrent *in situ* observations at each network. Stations with not-significant correlation at 0.05/0.01 confidence level are indicated by */** respectively. Gains of the downscaling procedure (G_EFFI, G_PREC, G_ACCU) at the 25 km scale with respect to the SMOS L3 are also shown. Bold indicates positive gain.

REMEDHUS	R	RMSD	cRMSD	bias	*a*	*b*	N	G_EFFI	G_PREC	G_ACCU
E10	0,71	0,103	0,056	-0,086	2,333	0,058	96	-0,121	-0,058	**0,005**
F6	0,39	0,081	0,070	0,041	0,650	-0,011	118	**0,036**	-0,052	**0,029**
H7	0,44	0,095	0,066	-0,068	3,629	-0,017	111	**0,107**	-0,204	**0,054**
H9	0,65	0,252	0,150	0,202	0,240	0,018	118	-0,009	-0,095	**0,102**
H13	0,78	0,047	0,043	0,018	0,901	-0,009	115	-0,221	**0,007**	**0,252**
I6	0,72	0,101	0,058	-0,082	4,212	0,033	122	-0,081	**0,011**	**0,013**
J3	0,69	0,093	0,054	-0,076	2,272	0,050	122	-0,070	-0,032	**0,006**
J12	0,77	0,181	0,046	0,176	0,779	-0,116	118	**0,020**	**0,065**	**0,027**
K4	0,71	0,086	0,054	-0,066	2,623	0,013	122	-0,050	-0,106	**0,004**
K9	0,29	0,073	0,071	0,018	0,401	0,045	118	-0,225	-0,082	**0,009**
K10	0,66	0,080	0,053	-0,060	1,576	0,037	118	-0,157	**0,081**	**0,030**
K13	0,75	0,115	0,048	0,105	0,752	-0,057	118	-0,144	**0,090**	**0,037**
L3	0,54	0,059	0,057	-0,015	1,254	-0,015	122	**0,194**	-0,012	**0,050**
L7	0,74	0,094	0,053	0,077	0,591	-0,011	118	**0,005**	**0,132**	**0,111**
M5 **	0,30	0,061	0,061	0,007	0,490	0,058	62	-0,422	-0,167	**0,313**
M9	0,70	0,085	0,045	0,071	0,739	-0,035	115	-0,097	**0,038**	**0,098**
M13	0,61	0,158	0,110	0,114	0,309	0,038	82	**0,058**	**0,044**	**0,168**
N9	0,63	0,073	0,051	0,053	0,665	-0,007	116	-0,057	**0,046**	**0,106**
O7	0,70	0,046	0,044	-0,012	0,898	0,020	118	**0,193**	**0,006**	-0,691
SMOSMANIA										
Barnas	0,52	0,076	0,043	0,063	0,476	0,023	65	**0,181**	**0,111**	**0,364**
Berzeme	0,65	0,090	0,049	0,075	0,639	-0,010	29	**0,318**	**0,280**	**0,077**
Condom	0,49	0,193	0,047	0,187	0,522	-0,049	81	-0,240	-0,130	-0,055
Creond	0,33	0,061	0,053	0,031	0,400	0,047	86	-0,380	-0,332	-0,213
Lahas	0,51	0,185	0,081	0,166	0,296	0,026	89	-0,063	-0,010	-0,132
Lezignan	0,66	0,045	0,041	-0,019	0,676	0,050	83	-0,390	-0,164	**0,567**
Mazan	0,53	0,130	0,100	0,083	0,197	0,063	65	**0,045**	**0,169**	**0,446**
Mejannes	0,60	0,116	0,079	0,086	0,303	0,050	95	-0,107	-0,126	**0,057**
Montaut	0,46	0,192	0,073	0,177	0,286	0,025	88	-0,112	-0,257	**0,009**
Mouthoumet	0,61	0,103	0,041	0,094	0,688	-0,034	98	-0,279	-0,143	-0,350
Narbonne	0,60	0,092	0,054	0,074	0,524	0,020	100	-0,247	**0,016**	-0,985
Peyrusse	0,57	0,146	0,052	0,137	0,491	-0,013	89	-0,198	-0,097	-0,135
Pezenas	0,56	0,059	0,056	0,017	0,615	0,048	101	-0,644	-0,243	**0,190**
Prades	0,59	0,079	0,056	0,056	0,526	0,041	100	-0,790	-0,139	-0,459
Sabres *	0,14	0,116	0,071	-0,091	0,096	0,105	76	**0,153**	**0,201**	-0,211
SaintFelix *	-0,23	0,135	0,061	0,120	-0,204	0,197	27	-0,783	-0,440	-0,134
Savenes	0,40	0,091	0,065	0,064	0,352	0,043	97	-0,221	-0,131	-0,386
Urgons	0,51	0,237	0,098	0,215	0,193	0,040	83	-0,106	-0,240	-0,068
Villevielle	0,62	0,107	0,086	0,064	0,272	0,063	92	-0,299	-0,122	-0,265
VAS										
Melbex1	0,77	0,042	0,035	0,024	0,686	0,008	107	-0,681	-0,089	-0,292
Melbex2	0,59	0,094	0,049	0,081	0,528	-0,015	102	-0,555	-0,225	-0,008

Table 5. Summary of the statistical metrics (R, RMSD, cRMSD, bias, slope *a* and intercept *b* of the linear regression, and number of observations N) for the individual comparisons between the SMOS L4 daytime concurrent *in situ* observations at each network. Stations with not-significant correlation at 0.05/0.01 confidence level are indicated by */** respectively.

REMEDHUS	R	RMSD	cRMSD	bias	*a*	*b*	N
E10	0,66	0,121	0,072	-0,098	2,153	0,062	103
F6	0,39	0,088	0,080	0,035	0,714	-0,016	131
H7	0,43	0,109	0,077	-0,077	3,198	0,000	120
H9	0,66	0,246	0,146	0,198	0,236	0,022	125
H13	0,67	0,063	0,060	0,020	0,882	-0,010	124
I6	0,63	0,107	0,072	-0,079	3,914	0,005	129
J3	0,67	0,095	0,057	-0,076	2,276	0,039	134
J12	0,69	0,182	0,059	0,173	0,767	-0,115	124
K4	0,68	0,086	0,056	-0,065	2,407	0,013	132
K9 **	0,23	0,085	0,084	0,011	0,252	0,061	123
K10	0,55	0,096	0,069	-0,067	1,523	0,039	127
K13	0,63	0,120	0,063	0,101	0,709	-0,049	128
L3	0,45	0,062	0,060	-0,015	1,008	0,003	132
L7	0,68	0,094	0,062	0,071	0,547	-0,005	123
M5	0,45	0,077	0,076	-0,011	0,655	0,044	68
M9	0,66	0,089	0,062	0,064	0,775	-0,038	117
M13	0,66	0,145	0,103	0,102	0,387	0,016	123
N9	0,58	0,084	0,068	0,049	0,738	-0,019	121
O7	0,64	0,064	0,062	-0,019	0,746	0,025	119
SMOSMANIA							
Barnas	0,50	0,080	0,044	0,066	0,537	0,010	76
Berzeme *	0,19	0,100	0,082	0,057	0,155	0,084	38
Condom *	0,15	0,206	0,094	0,184	0,522	-0,057	110
Creond **	0,22	0,075	0,070	0,025	0,495	0,033	107
Lahas	0,40	0,186	0,081	0,167	0,329	0,014	115
Lezignan	0,55	0,053	0,052	-0,012	0,619	0,048	103
Mazan	0,47	0,132	0,101	0,086	0,218	0,058	80
Mejannes	0,49	0,121	0,082	0,089	0,344	0,033	106
Montaut	0,48	0,198	0,073	0,184	0,354	0,000	104
Mouthoumet	0,48	0,106	0,055	0,091	0,721	-0,040	109
Narbonne	0,43	0,102	0,064	0,080	0,476	0,029	123
Peyrusse	0,45	0,151	0,065	0,136	0,481	-0,015	119
Pezenas	0,43	0,089	0,080	0,040	0,541	0,027	117
Prades	0,54	0,096	0,058	0,076	0,499	0,018	113
Sabres *	-0,32	0,109	0,103	-0,037	-0,583	0,238	12
SaintFelix *	-0,08	0,130	0,063	0,113	0,019	0,135	37
Savenes	0,32	0,090	0,067	0,060	0,372	0,041	116
Urgons	0,36	0,234	0,105	0,209	0,226	0,027	118
Villevielle	0,45	0,112	0,091	0,066	0,267	0,062	108
VAS							
Melbex1	0,67	0,055	0,049	0,025	0,750	-0,004	118
Melbex2	0,57	0,099	0,061	0,079	0,704	-0,041	113

Table 6. Summary of the statistical metrics (R, RMSD, cRMSD, bias, slope *a* and intercept *b* of the linear regression, and number of observations N) of the comparisons for the averaged soil moisture at each network and product. All correlations are significant at 0.01 confidence level.

L3	R	RMSD	cRMSD	bias	*a*	*b*	N
REMEDHUS	0,71	0,061	0,049	0,036	0,979	-0,037	182
SMOSMANIA	0,68	0,084	0,048	0,068	0,685	0,000	246
VAS	0,80	0,072	0,055	0,046	0,957	-0,046	90
L4 instant							
REMEDHUS	0,77	0,048	0,043	0,022	1,135	-0,037	115
SMOSMANIA	0,60	0,105	0,054	0,090	0,519	0,010	149
VAS	0,81	0,061	0,032	0,052	0,742	-0,022	86
L4 daytime							
REMEDHUS	0,67	0,063	0,060	0,020	0,957	-0,024	148
SMOSMANIA	0,51	0,109	0,062	0,090	0,565	-0,006	190
VAS	0,67	0,072	0,051	0,051	0,830	-0,032	131